Ferroelectric phase in Stockmayer fluids

B. Groh and S. Dietrich
Fachbereich Physik, Bergische Universität Wuppertal, 42097 Wuppertal, Federal Republic of Germany
(Received 1 April 1994)

By using a density-functional theory we establish the existence of a ferroelectric nematic phase in fluids consisting of spherical particles which interact with Lennard-Jones and dipolar forces. Our detailed analysis of the thermodynamic limit shows that for a polarized dipolar fluid within a single domain the free energy density depends on the shape of the sample as well as on the dielectric permittivity of the surrounding. For different aspect ratios of an ellipsoidal sample we determine the phase diagrams which comprise the isotropic gas and liquid phases and the ferroelectric liquid phase. For the latter we obtain the full probability distribution for the orientation of the particles. Its behavior in the vicinity of the phase transition between the isotropic and the ferroelectric liquid is analyzed by a Landau expansion of the grand-canonical potential. The repercussions of domain formation are briefly discussed.

PACS number(s): 64.70.−p, 77.80.−e, 64.60.Kw, 61.25.Em

I. INTRODUCTION

Molecular dynamics simulations of fluids consisting of either hard or soft dipolar spheres revealed the possibility that such systems can exhibit a ferroelectric nematic phase [1–4]. While it is well known that short-range steric interactions can induce orientational order in fluids without positional order [5,6], the numerical simulation by Wei and Patey represents the first contribution which shows that the dipolar interaction *alone* is capable of bringing about the formation of an orientationally ordered phase, which was already conjectured by Born in 1916 [7]. Moreover these authors showed that this phase is ferroelectric. On the other hand, it seems that the only experimental systems known up to now, which show a similar phase behavior, are certain ferroelectric liquid crystals exhibiting smectic phases [8,9]. Wei, Patey, and Perera also tried to understand their numerical findings on the basis of density-functional theory [10]. However, this analysis suffers both from a poor quantitative agreement with the simulation data and from difficulties in performing correctly the thermodynamic limit in these systems with long-range interactions. A mean-field theory for a dipolar lattice gas by Sano and Doi [11,12] gave further evidence for the existence of an orientationally ordered phase in dipolar fluids. One should also note the orientational instability observed by Kinoshita and Harada [13] as well as by Kasch and Forstmann [14] in solving the hypernetted-chain equations for dipolar hard spheres.

In the following we present a density-functional theory for Stockmayer fluids, which are somewhat more realistic in that they incorporate both the dispersion forces between the spherical particles as well as the dipolar interaction. Recently it has been demonstrated that the occurrence of the liquid-vapor phase separation is linked to a minimum admixture of dispersion forces [15,16]. This requirement is fulfilled for Stockmayer fluids, which may be used also to model ferrofluids, i.e., colloidal suspensions of small ferromagnetic particles [17]. Originally the present density-functional theory approach was designed to investigate the wetting behavior of such fluids in their isotropic phase [18] and has successfully been applied to analyze the properties of the interface between the isotropic liquid and vapor phases [19]. By applying this theory to the case of orientationally ordered fluid phases and by combining it with a careful analysis of the thermodynamic limit we find that a ferroelectric phase does indeed occur and that due to the long-range nature of the dipolar forces and the resulting depolarization effects the free energy density of this phase depends strongly on the shape of the sample. A needlelike volume is considerably more favorable for such phases than spherical volumes. This effect was not borne out by the previous analytical analyses mentioned above. In the molecular dynamics simulations a spherical volume was considered implicitly by using the Ewald summation technique [20]. These authors found, as we do, that the structural properties of such fluids also depend on the kind of dielectric surrounding them.

In contrast to Ref. [10] our density-functional theory does not rely on correlation functions that have to be obtained by independent methods. We are able to compute the *full* phase diagrams of these fluids for arbitrary aspect ratios of an ellipsoidal sample. They exhibit two isotropic and one ferroelectric phase. At high temperatures the isotropic and the ferroelectric phase are separated by a continuous phase transition, which turns into a first-order transition below a tricritical temperature. Close to the continuous phase transitions the anisotropies are small which allows us to carry out a systematic Landau expansion of the grand-canonical potential. This yields analytic expressions for the corresponding critical exponents and amplitudes. These critical exponents are mean-field-like; they are exact at the tricritical point.

Certain results of our approach have already been published in Ref. [21]. The purposes of the present contribution are to provide both additional results and further de-

tails as well as the derivation of our conclusions. In the following section we describe our model together with the approximations underlying the density-functional theory we use. The thermodynamic limit for different shapes of the sample is discussed in Sec. III, where we also analyze the relevance of a dielectric surrounding. Section IV deals with the determination of the thermodynamic state of the system. There we focus in particular on the orientational distribution in the ferroelectric phase. Section V is devoted to the phase diagrams. It turns out that the properties of oblate samples can be mapped exactly on those of appropriate elongated samples (Sec. VI). In Sec. VII we perform the systematic Landau expansion mentioned above. In Sec. VIII we discuss the possible consequences of domain formation. Our results are summarized in Sec. IX. Certain technical details are presented in Appendixes A and B.

II. DENSITY-FUNCTIONAL THEORY

In order to study the occurrence of ferroelectric nematic bulk phases and their thermodynamic and structural properties we resort to the density-functional theory worked out in Ref. [18]. Since such phases are characterized by long-range orientational order without long-range positional order the mean number density of particles at a point $\mathbf{r}$ and with orientation $\omega=(\theta,\phi)$ (see Fig. 1 in Ref. [18]) is given by

$$\hat{\rho}(\mathbf{r},\omega)=\rho\alpha(\omega)\ , \quad \int d\omega\,\alpha(\omega)=1\ , \tag{2.1}$$

where the angular distribution $\alpha(\omega)$ is normalized to 1 and ρ is the total mean number density without specified orientation. Thus we consider a single domain and we do not take into account spatial inhomogeneities near its surface.

As our model system we study Stockmayer fluids consisting of spherically shaped molecules interacting via a Lennard-Jones potential

$$w_{\mathrm{LJ}}(r_{12})=4\epsilon\left[\left[\frac{\sigma}{r_{12}}\right]^{12}-\left[\frac{\sigma}{r_{12}}\right]^{6}\right] \tag{2.2}$$

to which an interaction is added due to point dipoles embedded in spheres of diameter σ:

$$w_{\mathrm{dip}}(\mathbf{r},\mathbf{r}',\omega,\omega')=w_{\mathrm{dip}}(\mathbf{r}_{12}=\mathbf{r}-\mathbf{r}',\omega,\omega')$$
$$=\begin{cases}0, & r_{12}<\sigma\\ -\dfrac{m^2}{r_{12}^3}\left[\dfrac{3[\hat{\mathbf{m}}(\omega)\mathbf{r}_{12}][\hat{\mathbf{m}}(\omega')\mathbf{r}_{12}]}{r_{12}^2}-\hat{\mathbf{m}}(\omega)\hat{\mathbf{m}}(\omega')\right], & r_{12}>\sigma\ ;\end{cases} \tag{2.3}$$

m is the absolute value of the dipole moment and $\hat{\mathbf{m}}(\omega)$ a unit vector pointing in its direction. Thus the total pair potential is given by

$$w(\mathbf{r},\mathbf{r}',\omega,\omega')=w_{\mathrm{LJ}}(r_{12})+w_{\mathrm{dip}}(\mathbf{r},\mathbf{r}',\omega,\omega')\ . \tag{2.4}$$

According to Barker and Henderson [22] it is decomposed into a short-range repulsive reference part

$$w_{\mathrm{ref}}=\Theta(\sigma-r_{12})w_{\mathrm{LJ}}(r_{12}) \tag{2.5}$$

and a long-range attractive excess part

$$w_{\mathrm{ex}}(\mathbf{r},\mathbf{r}',\omega,\omega')=\Theta(r_{12}-\sigma)w(\mathbf{r},\mathbf{r}',\omega,\omega')\ . \tag{2.6}$$

The analysis of the quantitative consequences of applying either alternative separation schemes for the repulsive part of the interaction potential [23,24] or using the different approach of the so-called u expansion [25] is left to further studies.

Due to the translational invariance of $\hat{\rho}$ the approximate grand-canonical variational functional used in Ref. [18] reduces to

$$\frac{1}{V}\Omega[\rho,\{\alpha(\omega)\},T,\mu]$$
$$=f_{\mathrm{ref}}^{\mathrm{HS}}(\rho,T)+\frac{\rho}{\beta}\int d\omega\,\alpha(\omega)\ln[4\pi\alpha(\omega)]$$
$$+\frac{1}{V}\Omega_{\mathrm{int}}-\mu\rho\ . \tag{2.7}$$

V, T, and μ denote the volume of the fluid, its temperature, and its chemical potential, respectively. The first term in Eq. (2.7) is the free energy density of the reference system due to Carnahan and Starling [26]

$$f_{\mathrm{ref}}^{\mathrm{HS}}(\rho,T)=\frac{\rho}{\beta}\left[\ln(\rho\lambda^3)-1+\frac{4\eta-3\eta^2}{(1-\eta)^2}\right], \tag{2.8}$$

where λ denotes the thermal de Broglie wavelength and $\eta=(\pi/6)d^3\rho$ the packing fraction with a temperature dependent diameter d, as given by Barker and Henderson [27], accounting for the soft sphere character of the reference fluid:

$$d(T)=\int_0^{\sigma}dr(1-e^{-\beta w_{\mathrm{ref}}(r)})\ . \tag{2.9}$$

The second contribution to the grand-canonical functional stems from the additional entropy due to the orientational degrees of freedom. It vanishes for the isotropic fluid for which $\alpha(\omega)=1/4\pi$. The interaction contribution

$$\Omega_{\mathrm{int}}=\frac{\rho^2}{2\beta}\int_V d^3r\int_V d^3r'\int d\omega\,d\omega'\alpha(\omega)\alpha(\omega')e^{-\beta w_{\mathrm{ref}}(\mathbf{r},\mathbf{r}')}$$
$$\times(1-e^{-\beta w_{\mathrm{ex}}(\mathbf{r},\mathbf{r}',\omega,\omega')}) \tag{2.10}$$

follows from using [18] the low-density approximation for the pair distribution function:

$$g^{(2)}_{\rm app}(\mathbf{r},\mathbf{r}',\omega,\omega')=e^{-\beta w(\mathbf{r},\mathbf{r}',\omega,\omega')} . \tag{2.11}$$

For uniaxial molecules the angular distribution $\alpha(\omega)$ depends only on the angle θ and thus allows for the following expansion in Legendre polynomials:

$$\begin{aligned} 2\pi\alpha(\omega)&=\bar{\alpha}(\cos\theta)=\sum_{l=0}^{\infty}\alpha_l P_l(\cos\theta) , \\ \alpha_l&=\frac{2l+1}{2}\int_{-1}^{1}dx\,\bar{\alpha}(x)P_l(x) , \end{aligned} \tag{2.12}$$

where $\alpha_0=\frac{1}{2}$ due to the normalization introduced in Eq. (2.1). In order to proceed we express the Mayer function of the excess intermolecular potential

$$\tilde{f}(\mathbf{r}_{12},\omega,\omega')=e^{-\beta w_{\rm ex}(\mathbf{r}_{12},\omega,\omega')}-1 \tag{2.13}$$

in terms of the rotational invariants

$$\begin{aligned} \Phi_{l_1l_2l}(\omega,\omega',\omega_{12})=&\sum_{m_1,m_2,m}{}' C(l_1l_2l,m_1m_2m)Y_{l_1m_1}(\omega) \\ &\times Y_{l_2m_2}(\omega')Y^{*}_{lm}(\omega_{12}) \end{aligned} \tag{2.14}$$

with

$$\sum_{m_1,m_2,m}{}' = \sum_{m_1=-l_1}^{l_1}\sum_{m_2=-l_2}^{l_2}\sum_{m=-l}^{l} ; \tag{2.15}$$

$C(l_1l_2l,m_1m_2m)$ are Clebsch-Gordan coefficients using the convention of Rose [28] and Gray and Gubbins [29] and $(l_1l_2l)=\Lambda\in\mathbb{N}_0^3$. These functions are a complete set of orthogonal functions of ω, ω', and ω_{12} that are invariant under simultaneous rotations of these three solid angles. In Ref. [18] analytical expressions for the first expansion coefficients in the series

$$\tilde{f}(\mathbf{r}_{12},\omega,\omega')=\sum_{\Lambda}\hat{f}_\Lambda\Phi_\Lambda \tag{2.16}$$

up to $(l_1l_2l)=(224)$ have been derived. The behavior of the coefficients $\hat{f}_\Lambda$ for large r_{12} can be obtained by expanding the exponential in Eq. (2.13). Since for $r_{12}\geq\sigma$

$$\begin{aligned} w_{\rm ex}(\mathbf{r},\mathbf{r}',\omega,\omega')&=w_{\rm LJ}(r_{12})+w_{\rm dip}(\mathbf{r},\mathbf{r}',\omega,\omega') \\ &=w_{\rm LJ}(r_{12}) \\ &\quad-\frac{m^2}{r_{12}^3}(4\pi)^{3/2}\sqrt{\tfrac{2}{15}}\Phi_{112}(\omega,\omega',\omega_{12}) \end{aligned} \tag{2.17}$$

and [see Eq. (B1) in Ref. [18]]

$$\hat{f}_\Lambda(r_{12})=\frac{4\pi}{2l+1}\int d\omega\,d\omega'\tilde{f}(r_{12},\omega,\omega',\omega_{12})\Phi^{*}_\Lambda(\omega,\omega',\omega_{12}) ,$$
$$\Lambda=(l_1l_2l) , \tag{2.18}$$

all $\hat{f}_\Lambda$ with $\Lambda\neq(112)$ decay for large r_{12} as r_{12}^{-n}, $n\geq 6$. For $\Lambda=(112)$, however, one has $\hat{f}_{112}(r_{12}\to\infty)\sim r_{12}^{-3}$.

III. THERMODYNAMIC LIMIT AND SHAPE DEPENDENCE

A. Thermodynamic limit

In order to extract the system size we introduce the sum and the difference of the coordinates in the two positional integrals of the interaction contribution to Ω [see Eq. (2.10)]:

$$\mathbf{r}_{12}=\mathbf{r}-\mathbf{r}' , \quad \mathbf{r}_S=\tfrac{1}{2}(\mathbf{r}+\mathbf{r}') . \tag{3.1}$$

If the volume V exhibits inversion symmetry about the center of the volume chosen as the origin, one finds the identities

$$\begin{aligned} &\{\mathbf{r}_{12}\in\mathbb{R}^3|\mathbf{r}_{12}=\mathbf{r}-\mathbf{r}'\wedge\mathbf{r}\in V\wedge\mathbf{r}'\in V\} \\ &\qquad=\{\mathbf{r}\in\mathbb{R}^3|\tfrac{1}{2}\mathbf{r}\in V\}\equiv 2V \end{aligned} \tag{3.2}$$

and (see Fig. 1) for fixed $\mathbf{r}_{12}$

$$\begin{aligned} &\{\mathbf{r}_S\in\mathbb{R}^3|\mathbf{r}_S=\tfrac{1}{2}(\mathbf{r}+\mathbf{r}')\wedge\mathbf{r}\in V\wedge\mathbf{r}'\in V\} \\ &\qquad=V_+(\mathbf{r}_{12})\cap V_-(\mathbf{r}_{12})\equiv V_S(\mathbf{r}_{12}) , \end{aligned} \tag{3.3}$$

where

$$V_\pm(\mathbf{r}_{12})=\{\mathbf{r}_\pm\in\mathbb{R}^3|\mathbf{r}_\pm=\mathbf{r}\pm\tfrac{1}{2}\mathbf{r}_{12}\wedge\mathbf{r}\in V\} . \tag{3.4}$$

For integrands that do not depend on $\mathbf{r}_S$, such as that in Eq. (2.10), one obtains

$$\begin{aligned} \frac{1}{V}\int_V d^3r\int_V d^3r'\cdots&=\frac{1}{V}\int_{2V}d^3r_{12}\int_{V_S(\mathbf{r}_{12})}d^3r_S\cdots \\ &=\int_{2V}d^3r_{12}\frac{V_S(\mathbf{r}_{12})}{V}\cdots . \end{aligned} \tag{3.5}$$

Now we restrain ourselves to the case of a rotational ellipsoid with two equal axes of length R and one axis of length kR. The preferred orientation of the ferroelectric phase, i.e., the director, is assumed to be along the latter axis. [This assumption is supported by macroscopic considerations (see Sec. III B).] Thus the angle θ in Eq. (2.12) is measured relative to this axis (see Fig. 1).

Inserting Eqs. (2.16) and (2.14) into Eq. (2.10) and performing one spatial integration leads to the following expression for the interaction contribution:

$$\begin{aligned} \frac{1}{V}\Omega_{\rm int}=&-\frac{1}{4\pi^2}\frac{\rho^2}{2\beta}\sum_{l_1,l_2,l}\int_{2V\setminus S_\sigma}d^3r_{12}\,h\left(\theta_{12},\frac{r_{12}}{2R}\right)\hat{f}_{l_1l_2l}(r_{12}) \\ &\times\int d\omega\,d\omega'\alpha_{l_1}\alpha_{l_2}P_{l_1}(\cos\theta)P_{l_2}(\cos\theta') \\ &\times\sum_{m_1,m_2,m}{}' C(l_1l_2l,m_1m_2m)Y_{l_1m_1}(\omega)Y_{l_2m_2}(\omega')Y^{*}_{lm}(\omega_{12}) \end{aligned} \tag{3.6}$$

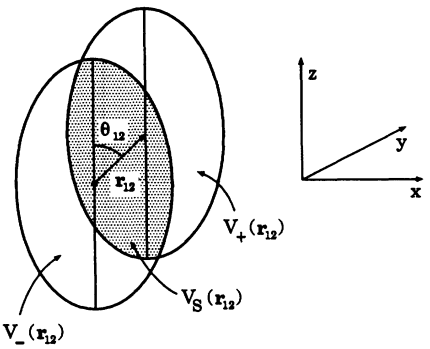

FIG. 1. Illustration of the regions of integration in Eq. (3.5). For an ellipsoidal sample and a fixed vector difference $\mathbf{r}_{12}$ the vector sum $\mathbf{r}_S$ lies in the shaded volume $V_S(\mathbf{r}_{12})$ given by the intersection $V_+(\mathbf{r}_{12})\cap V_-(\mathbf{r}_{12})$ of two ellipsoids.

with $S_\sigma=\{\mathbf{r}\in\mathbb{R}^3|r<\sigma\}$ and where

$$h\left[\theta_{12},\frac{r_{12}}{2R}\right]=\frac{V_S(\mathbf{r}_{12})}{V} \tag{3.7}$$

is independent of ϕ_{12} and depends on r_{12} only via the dimensionless ratio $r_{12}/2R$. Because of $P_l(\cos\theta)=\sqrt{4\pi/(2l+1)}Y_{l0}(\omega)$, the orthogonality of the spherical harmonics, and the properties of the Clebsch-Gordan coefficients, all terms with $m_1\neq 0$, $m_2\neq 0$, or $m\neq 0$, vanish.

Thus one obtains

$$\frac{1}{V}\Omega_{\text{int}}=-\frac{\rho^2}{\beta}\frac{1}{\sqrt{4\pi}}\sum_{l_1,l_2,l}\left[\frac{2l+1}{(2l_1+1)(2l_2+1)}\right]^{1/2}\times C(l_1l_2l,000)\alpha_{l_1}\alpha_{l_2}I_{l_1l_2l} \tag{3.8}$$

with

$$I_{l_1l_2l}=\int_0^\pi d\theta_{12}\sin\theta_{12}P_l(\cos\theta_{12})\times\int_\sigma^{2Rg(\theta_{12})}dr_{12}r_{12}^2\hat{f}_{l_1l_2l}(r_{12})h\left[\theta_{12},\frac{r_{12}}{2R}\right]. \tag{3.9}$$

The function

$$g(\theta_{12})=\frac{r_{12,\max}(\theta_{12})}{2R}, \tag{3.10}$$

where $r_{12,\max}(\theta_{12})$ defines the surface of $2V$, can be determined by using the parametrization of the ellipse

$$\mathbf{x}(t)=2R(\sin t,k\cos t), \tag{3.11}$$

and $\cos\theta=[\mathbf{x}(t)\cdot\mathbf{e}_2]/|\mathbf{x}(t)|$, leading to $\tan^2 t=k^2\tan^2\theta$ and

$$g(\theta)=\frac{|\mathbf{x}|}{2R}=\left[\sin^2\theta+\frac{1}{k^2}\cos^2\theta\right]^{-1/2}. \tag{3.12}$$

In order to determine the function h we calculate the volume V_S given by the intersection of two ellipsoids displaced relative to each other by the vector $\mathbf{r}_{12}$ (see Fig. 1). For a sphere ($k=1$) the volume V_S is twice that of a cap of a sphere so that one has

$$h_{\text{sph}}(\gamma)=1-\tfrac{3}{2}\gamma+\tfrac{1}{2}\gamma^3,\quad \gamma=\frac{r_{12}}{2R}, \tag{3.13}$$

which is independent of θ. The general problem for ellipsoids can be mapped onto the one for a sphere by the dilation $z\mapsto z'=z/k$, which leads to

$$V_S^{\text{ell}}(r_{12},\theta)=kV_S^{\text{sph}}\left[r'_{12}=r_{12}\left[\sin^2\theta+\frac{1}{k^2}\cos^2\theta\right]^{1/2}\right]. \tag{3.14}$$

Since the volume of the full ellipsoid is k times the volume of the full sphere with radius R one finds

$$\begin{aligned}h_{\text{ell}}(\theta,\gamma)&=h_{\text{sph}}\left[\gamma'=\frac{r_{12}}{2R}\left[\sin^2\theta+\frac{1}{k^2}\cos^2\theta\right]^{1/2}\right]\\&=1-\tfrac{3}{2}\gamma\left[\sin^2\theta+\frac{1}{k^2}\cos^2\theta\right]^{1/2}+\tfrac{1}{2}\gamma^3\left[\sin^2\theta+\frac{1}{k^2}\cos^2\theta\right]^{3/2}\\&=1+h_1(\theta)\gamma+h_3(\theta)\gamma^3.\end{aligned} \tag{3.15}$$

In the next step we insert Eq. (3.15) and the asymptotic expansion

$$\hat{f}_\Lambda(r\to\infty)=\sum_{i=3}^{\infty}c_i^{(\Lambda)}r^{-i} \tag{3.16}$$

into Eq. (3.9) and regroup the terms according to their power of r:

$$I_\Lambda=\int_0^\pi d\theta\sin\theta P_l(\cos\theta)\int_\sigma^{2Rg(\theta)}dr\left[r^2\frac{c_3^{(\Lambda)}h_3(\theta)}{(2R)^3}+r\frac{c_4^{(\Lambda)}h_3(\theta)}{(2R)^3}+\left[\frac{c_3^{(\Lambda)}h_1(\theta)}{2R}+\frac{c_5^{(\Lambda)}h_3(\theta)}{(2R)^3}\right]+r^{-1}\left[c_3^{(\Lambda)}+\frac{c_4^{(\Lambda)}h_1(\theta)}{2R}+\frac{c_6^{(\Lambda)}h_3(\theta)}{(2R)^3}\right]+\sum_{i=2}^{\infty}r^{-i}\left[c_{i+2}^{(\Lambda)}+\frac{c_{i+3}^{(\Lambda)}h_1(\theta)}{2R}+\frac{c_{i+5}^{(\Lambda)}h_3(\theta)}{(2R)^3}\right]\right]. \tag{3.17}$$

The thermodynamic limit $R\to\infty$ will now be considered in two cases. First, if $\Lambda\neq(112)$ one has $c_3^{(\Lambda)}=0$ (see Sec. II) and therefore

$$\lim_{R\to\infty} I_\Lambda = \int_0^\pi d\theta \sin\theta P_l(\cos\theta) \sum_{i=2}^{\infty} \frac{1}{i-1} \frac{1}{\sigma^{i-1}} c_{i+2}^{(\Lambda)}$$
$$= \int_{-1}^{1} dx\, P_l(x) \int_\sigma^\infty dr\, r^2 \hat{f}_\Lambda(r) = 2\delta_{l,0}\delta_{l_1,l_2} \int_\sigma^\infty dr\, r^2 \hat{f}_{l_1 l_1 0}(r) \,. \tag{3.18}$$

Note that, due to the triangle condition for the first three arguments of the Clebsch-Gordan coefficients in Eq. (2.14), $l=0$ implies that they vanish unless $l_1=l_2$. Second, if $\Lambda=(112)$ all those terms that contribute to Eq. (3.18) vanish because $l\neq 0$. Since $c_3^{(112)}\neq 0$ one therefore has

$$\lim_{R\to\infty} I_{112} = \lim_{R\to\infty} c_3^{(112)} \int_0^\pi d\theta \sin\theta P_2(\cos\theta) \int_\sigma^{2Rg(\theta)} dr \left| r^2 \frac{h_3(\theta)}{(2R)^3} + \frac{h_1(\theta)}{2R} + r^{-1} \right|$$
$$= c_3^{(112)} \int_0^\pi d\theta \sin\theta P_2(\cos\theta) [\tfrac{1}{3} h_3(\theta) g(\theta)^3 + h_1(\theta) g(\theta) + \ln g(\theta)] \,. \tag{3.19}$$

Due to the form of the functions $h_i(\theta)$ [Eq. (3.15)] and $g(\theta)$ [Eq. (3.12)] the first two terms vanish and one is left with the shape dependent (i.e., dependent on k) expression

$$I(k) = \frac{I_{112}}{c_3^{(112)}} = -\int_0^1 dx\, P_2(x) \ln[k^2(1-x^2)+x^2]$$
$$= \begin{cases} \dfrac{k^2+2}{3(k^2-1)} - \dfrac{k}{(k^2-1)^{3/2}} \ln(k+\sqrt{k^2-1}) \,, & k \geq 1 \\ \dfrac{k^2+2}{3(k^2-1)} + \dfrac{k}{(1-k^2)^{3/2}} \arctan\dfrac{\sqrt{1-k^2}}{k} \,, & k \leq 1 \,. \end{cases} \tag{3.20}$$

This function is shown in Fig. 2. It is a monotonically increasing function of k with $I(k\to 0) = -\frac{2}{3} + (\pi/2)k - 2k^2 + \cdots$, $I(k=1)=0$, and $I(k\to\infty) = \frac{1}{3} - (\ln k/k^2 + \cdots$. The value of $c_3^{(112)}$ can be inferred from Eq. (B34) in Ref. [18] yielding

$$c_3^{(112)} = 8\pi \left[\frac{2\pi}{15}\right]^{1/2} \beta m^2 \,. \tag{3.21}$$

By inserting Eqs. (3.18), (3.19), and (3.21) into Eq. (3.8) the thermodynamic limit of the interaction contribution to the grand-canonical potential reads ($C(l_1 l_2 0,000) = (-1)^{l_1}(2l_1+1)^{-1/2}\delta_{l_1,l_2}$ and $C(112,000) = \sqrt{\frac{2}{3}}$ [see Eqs. (A.157) and (A.162) in Ref. [29])

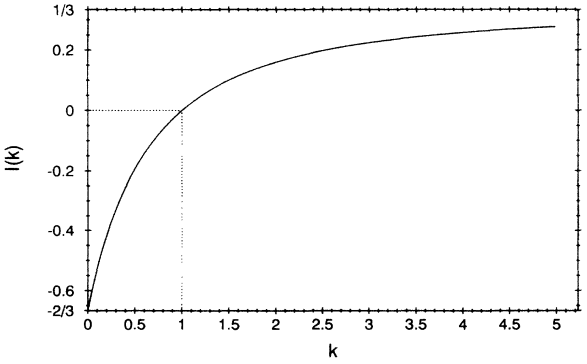

FIG. 2. The function $I(k)$ [see Eq. (3.20)] which determines the shape dependence of the grand-canonical potential; $I(0) = -\frac{2}{3}$, $I(1)=0$, and $I(\infty)=\frac{1}{3}$. $\frac{1}{3} - I(k)$ is the usual depolarization factor of a rotational ellipsoid with aspect ratio k. $k<1$ corresponds to oblate and $k>1$ to elongated samples.

$$\lim_{V\to\infty} \frac{1}{V} \Omega_{\rm int} = \rho^2 \sum_{l=0}^{\infty} u_l \alpha_l^2 \,, \tag{3.22}$$

where

$$u_l = -\frac{1}{\beta} \frac{(-1)^l}{\sqrt{\pi}(2l+1)^{3/2}} \int_\sigma^\infty dr_{12} r_{12}^2 \hat{f}_{ll0}(r_{12}), \quad l\neq 1 \tag{3.23}$$

and

$$u_1 = \frac{1}{\beta} \frac{1}{\sqrt{\pi} 3^{3/2}} \int_\sigma^\infty dr_{12} r_{12}^2 \hat{f}_{110}(r_{12}) - \frac{8\pi}{9} I(k) m^2 \,. \tag{3.24}$$

The last term in Eq. (3.24) contains the whole shape dependence of the grand-canonical potential.

By using a similar density-functional theory for dipolar fluids Wei, Patey, and Perera [10] stated that the grand-canonical potential would not be well defined in the thermodynamic limit "without exactly specifying how the long-range dipolar forces are treated." They introduced a cutoff short-range potential and treated the region outside the cutoff sphere as a dielectric continuum. *After* calculating the thermodynamic limit of that grand-canonical functional they replaced the cutoff radius R_C by infinity and arrived at a result which depends on the dielectric constant of the surrounding medium, but *not* on the sample shape. Thus the order in which the two limits $V\to\infty$ and $R_C\to\infty$ are taken is important, because our shape dependent results correspond to performing the limit $R_C\to\infty$ first, thereby recovering the original dipolar interaction potential, and then $V\to\infty$ for fixed shape. Obviously for an actual dipolar fluid this latter approach is the appropriate one yielding a well defined thermodynamic limit.

B. Electrostatic energy density and dielectric surrounding media

The above considerations apply to the case that the dipolar liquid within the ellipsoid is surrounded by vacuum. However, in an actual experimental situation the liquid will be contained by a solid material. If the liquid does not exhibit a net polarization, the nature of the container will only enter into the *surface* contribution to the free energy of the liquid. If, however, the liquid is in a ferroelectric state, the container will be polarized too and thus in turn give rise to a reaction field $\mathbf{E}_{RF}$ within the fluid. This leads to a contribution to the *bulk* free energy so that the bulk properties of the ferroelectric liquid will depend on the nature of the container.

In order to extend the results in Eqs. (3.22)–(3.24) to this more general case we recall that the shape dependence of the free energy of dipolar systems, which is a consequence of the long-range nature of the dipolar interaction, has already been known for a long time; e.g., the shape dependence of the specific heat of dipolar magnets has been verified experimentally by Levy and Landau in 1968 [30]. Macroscopically this shape dependence can be understood by considering the electric field inside a homogeneously polarized ellipsoid embedded in vacuum. For a rotationally symmetric ellipsoid with polarization $\mathbf{P}$ the corresponding electric field is given by [31,32]

$$E_i = -4\pi D_i(k) P_i \ , \quad i=1,2,3 \tag{3.25}$$

where (see, e.g., p. 56 in Ref. [32])

$$D_3(k)\equiv D(k) = -\frac{1}{k^2-1} + \frac{k}{(k^2-1)^{3/2}} \ln(k+\sqrt{k^2-1}) = \frac{1}{3} - I(k) \geq 0 \tag{3.26}$$

is the depolarization factor along the symmetry axis and

$$D_1(k) = D_2(k) = \frac{1-D(k)}{2} \ . \tag{3.27}$$

Inter alia the free energy of the polarized liquid must contain the corresponding electrostatic energy density

$$\frac{W(k)}{V} = -\tfrac{1}{2}\mathbf{P}\cdot\mathbf{E} = 2\pi\left[\frac{1-D(k)}{2}(P_1^2+P_2^2)+D(k)P_3^2\right] = 2\pi\{D(k)P^2+\tfrac{1}{2}[1-3D(k)](P_1^2+P_2^2)\} \ , \tag{3.28}$$

where $P^2 = P_1^2+P_2^2+P_3^2$. For fixed absolute value P the electrostatic energy is minimal if $P_1=P_2=0$, as long as $D(k)<\frac{1}{3}$, i.e., for aspect ratios $k>1$. Thus in this case one expects that the polarization points along the long axis and that the orientational distribution $\alpha(\omega)$ depends only on the angle θ due to the symmetry of the problem as assumed above. Then, since $\mathbf{P}=P_3\mathbf{e}_3$ with $P_3 = \int d\hat{\omega}\,\hat{\rho}(\mathbf{r},\omega) m\cos\theta = \rho m \int_{-1}^{1} dx\, x\bar{\alpha}(x) = \frac{2}{3}\rho m \alpha_1$, one has

$$\frac{W(k)}{V} = \frac{8\pi}{27}\rho^2 m^2 \alpha_1^2 - \frac{8\pi}{9} I(k) \rho^2 m^2 \alpha_1^2 \ . \tag{3.29}$$

Thus the shape dependent contributions $\sim I(k)$ in $\lim_{V\to\infty}(1/V)\Omega_{\text{int}}$ and $W(k)/V$ are the same.

On the other hand, for oblate ellipsoids ($k<1$) one expects that the polarization vector spontaneously chooses one particular direction within the xy plane, leading again to a minimum in Eq. (3.28). This case will be discussed in Sec. VI. In the following we focus on the case $k>1$.

If the polarized liquid is surrounded by a container characterized by a dielectric constant ϵ, the induced polarization in the container generates the reaction field

$$\mathbf{E}_{RF} = -4\pi D(k)\frac{(\epsilon-1)[1-D(k)]}{(\epsilon-1)D(k)-\epsilon}\mathbf{P} \tag{3.30}$$

so that the total internal field as the sum of the depolarization and the reaction field is [33]

$$\mathbf{E} = -4\pi\frac{D(k)}{\epsilon-D(k)(\epsilon-1)}\mathbf{P} \ , \tag{3.31}$$

which reduces to Eq. (3.25) for $\epsilon=1$ and for $P_1=P_2=0$ (see above). The resulting electrostatic energy density

$$\frac{1}{V}W(k,\epsilon) = 2\pi\frac{D(k)}{\epsilon-D(k)(\epsilon-1)}P^2 \tag{3.32}$$

[see Eq. (3.28)] decreases monotonically as function of k or ϵ and vanishes for $k\to\infty$ or $\epsilon\to\infty$. In the latter case the surrounding medium is effectively conducting so that the charges at the container surface will always arrange themselves in such a way that there is no electric field inside the sample [see Eq. (3.31)]. Thus for $\epsilon\to\infty$ the bulk properties of the ferroelectric fluid become independent of the shape of the sample.

We argue that, in order to take the effect of the polarization of the container into account, the grand-canonical potential density must be augmented by

$$\frac{1}{V}[W(k,\epsilon)-W(k,\epsilon=1)] = -\tfrac{1}{2}\mathbf{P}\cdot\mathbf{E}_{RF} \ . \tag{3.33}$$

This leads us to the final expression

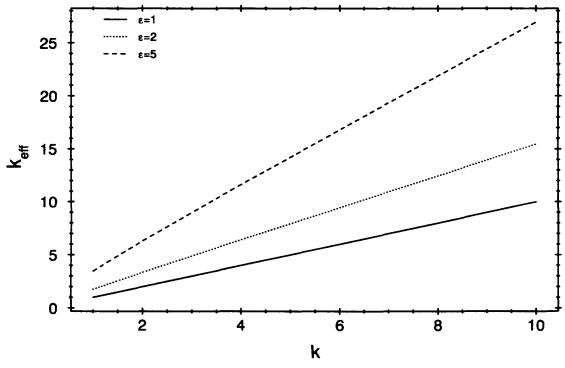

FIG. 3. The effective aspect ratio k_{eff} defined in Eq. (3.35) as a function of the actual aspect ratio k for different dielectric constants ϵ of the surrounding medium. A sample with aspect ratio k_{eff} surrounded by vacuum has the same free energy density as a sample with aspect ratio k surrounded by a dielectric continuum, $k_{\text{eff}}(k,\epsilon=1)=k$.

$$\lim_{V\to\infty}\frac{1}{V}\Omega_{\rm int}=\rho^2\sum_{l=0}^{\infty}\hat{u}_l\alpha_l^2-\frac{8\pi}{9}m^2\rho^2\alpha_1^2 \times\left[I(k)-D(k)\frac{(\epsilon-1)[D(k)-1]}{\epsilon-D(k)(\epsilon-1)}\right], \tag{3.34}$$

where $\hat{u}_{l\neq1}=u_l$ and $\hat{u}_1=1/(\beta\sqrt{\pi}3^{3/2})\int_\sigma^\infty dr\, r^2\hat{f}_{110}(r)$. (In Eq. (3.34) the term in square brackets can be rewritten as $\frac{1}{3}-D(k)/[\epsilon-D(k)(\epsilon-1)]$.) With the definition

$$I(k)-D(k)\frac{(\epsilon-1)[D(k)-1]}{\epsilon-D(k)(\epsilon-1)}=I[k_{\rm eff}(k,\epsilon)], \tag{3.35}$$

one sees that for any k a system with $\epsilon\neq1$ can be mapped onto the case $\epsilon=1$ by rescaling the axis ratio from k to $k_{\rm eff}(k,\epsilon)\geq k$. As can be seen in Fig. 3 a larger value of ϵ corresponds to a larger value of $k_{\rm eff}$. Therefore, in the following, we confine our analysis to the case $\epsilon=1$.

IV. THERMODYNAMIC STATES

Only the constants u_0, u_1, and u_2 in Eq. (3.22) are known from Ref. [18]. But a cutoff of the summation after the term $l=2$ would mean that the function $\bar{\alpha}(x)$ is approximated by a linear combination of the first three Legendre polynomials, i.e., a quadratic function in $x=\cos\theta$. Since in the ordered phase this function turns out to be strongly peaked at $x=1$ (or $x=-1$), this would be a bad approximation.

As an alternative we pursue an approach which takes into account the whole function $\bar{\alpha}(x)$. To this end Eq. (2.12) is inserted into Eq. (3.22) and gives

$$\lim_{V\to\infty}\frac{1}{V}\Omega_{\rm int}=\rho^2\sum_{l=0}^{\infty}u_l\left[\left(\frac{2l+1}{2}\right)\int_{-1}^{1}dx\,P_l(x)\bar{\alpha}(x)\right]^2 =\frac{\rho^2}{2}\int_{-1}^{1}dx\int_{-1}^{1}dx'\bar{\alpha}(x)\bar{\alpha}(x')K(x,x'), \tag{4.1}$$

where

$$K(x,x')=\sum_{l=0}^{\infty}\frac{(2l+1)^2}{2}u_lP_l(x)P_l(x'). \tag{4.2}$$

By using Eqs. (3.23) and (2.18) the coefficients u_l can be expressed as

$$u_l=-\frac{1}{\beta}\frac{4\sqrt{\pi}(-1)^l}{(2l+1)^{3/2}} \times\int_\sigma^\infty dr_{12}r_{12}^2\int d\omega\,d\omega'\tilde{f}(r_{12},\omega,\omega',\omega_{12}) \times\Phi^*_{ll0}(\omega,\omega',\omega_{12}) -\frac{8\pi}{9}I(k)m^2\delta_{l,1}. \tag{4.3}$$

[Note that in Eq. (4.3) the spatial integration is carried out *after* the angular integrations.] Due to the five remaining integrations it would be a difficult task to calculate u_l numerically as function of T and m. Therefore we expand the Mayer function $\tilde{f}$ and the coefficients u_l for small dipole moments:

$$\tilde{f}=-1+e^{-\beta w_{\rm LJ}}[1-\beta w_{\rm dip}+\tfrac{1}{2}(\beta w_{\rm dip})^2 -\tfrac{1}{6}(\beta w_{\rm dip})^3+\tfrac{1}{24}(\beta w_{\rm dip})^4+\cdots] \tag{4.4}$$

and

$$u_l=u_l^{(0)}+u_l^{(2)}m^2+u_l^{(4)}m^4+u_l^{(6)}m^6+u_l^{(8)}m^8+\cdots. \tag{4.5}$$

As will be shown below [see Eq. (A14)] only terms of order m^p with $p\geq2l$ contribute to u_l. This means that if one is interested in contributions to $\Omega_{\rm int}$ up to terms proportional to m^{2L}, the infinite series in Eq. (4.2) can be truncated such that $u_{l>L}=0$. Within this expansion the angular integrations in Eq. (4.3) can be performed term by term using the orthogonality relation of the rotational invariants Φ_Λ [29]:

$$\int d\omega\,d\omega'\Phi_\Lambda(\omega,\omega',\omega_{12})\Phi^*_{\Lambda'}(\omega,\omega',\omega_{12})=\frac{2l+1}{4\pi}\delta_{\Lambda,\Lambda'}. \tag{4.6}$$

The zeroth-order term is [$\Phi_{000}=(4\pi)^{-3/2}$]

$$u_l^{(0)}=\frac{8\pi}{\beta}\delta_{l,0}\int_\sigma^\infty dr\,r^2(1-e^{-\beta w_{\rm LJ}(r)}). \tag{4.7}$$

For the higher-order terms in Eq. (4.5) it is useful to apply Eq. (2.17). Obviously the shape independent contribution proportional to m^2 is zero. However, the shape dependent contribution is nonzero and proportional to m^2 so that

$$u_l^{(2)}=-\frac{8\pi}{9}I(k)\delta_{l,1}. \tag{4.8}$$

The expressions for the terms $u_l^{(4)}$, $u_l^{(6)}$, and $u_l^{(8)}$ are derived in Appendixes A and B leading to the results

$$u_0=\frac{8\pi}{\beta}\int_\sigma^\infty dr\,r^2(1-e^{-\beta w_{\rm LJ}(r)})-\frac{8\pi}{3}\frac{\beta m^4}{\sigma^3}I_4(\beta\epsilon) -\frac{8\pi}{25}\frac{\beta^3m^8}{\sigma^9}I_{10}(\beta\epsilon)+O(m^{12}), \tag{4.9}$$

$$u_1=-\frac{8\pi}{9}I(k)m^2-\frac{16\pi}{225}\frac{\beta^2m^6}{\sigma^6}I_7(\beta\epsilon)+O(m^{10}), \tag{4.10}$$

$$u_2=-\frac{8\pi}{375}\frac{\beta m^4}{\sigma^3}I_4(\beta\epsilon)-\frac{32\pi}{6125}\frac{\beta^3m^8}{\sigma^9}I_{10}(\beta\epsilon)+O(m^{12}), \tag{4.11}$$

$$u_3=\frac{16\pi}{25\,725}\frac{\beta^2m^6}{\sigma^6}I_7(\beta\epsilon)+O(m^{10}), \tag{4.12}$$

$$u_4=-\frac{8\pi}{99\,225}\frac{\beta^3m^8}{\sigma^9}I_{10}(\beta\epsilon)+O(m^{12}). \tag{4.13}$$

All contributions $u_{l>4}$ vanish in this order. The dimensionless integrals I_n are defined as

$$I_n(y)=\int_1^\infty dx\,x^{-n}e^{4y(x^{-6}-x^{-12})}. \tag{4.14}$$

The equilibrium configuration for given T and μ is determined by minimizing the total grand-canonical functional with respect to ρ and the function $\bar{\alpha}(x)$:

$$\frac{1}{V}\frac{\partial\Omega}{\partial\rho}=\mu_{\rm HS}(\rho,T)+\frac{1}{\beta}\int_{-1}^{1}dx\,\bar{\alpha}(x)\ln[2\bar{\alpha}(x)]$$
$$+2\rho\sum_{l=0}^{\infty}u_l\alpha_l^2-\mu=0 \tag{4.15}$$

and

$$\frac{\delta}{\delta\bar{\alpha}}\left[\frac{\Omega}{V}+\kappa\left[1-\int_{-1}^{1}dx\,\bar{\alpha}(x)\right]\right]$$
$$=\frac{\delta}{\delta\bar{\alpha}}\left[\frac{\Delta\Omega}{V}+\kappa\left[1-\int_{-1}^{1}dx\,\bar{\alpha}(x)\right]\right]=0\ . \tag{4.16}$$

Here

$$\frac{1}{V}\Delta\Omega[\rho,\{\bar{\alpha}(x)\},T]$$
$$=\frac{\rho}{\beta}\int_{-1}^{1}dx\,\bar{\alpha}(x)\ln[2\bar{\alpha}(x)]+\rho^2\sum_{l=1}^{\infty}u_l\alpha_l^2 \tag{4.17}$$

denotes the $\bar{\alpha}$ dependent part of Ω which vanishes in the isotropic phase. $\mu_{\rm HS}(\rho)=\partial f_{\rm ref}^{\rm HS}/\partial\rho$ is the chemical potential of the reference system and κ a Lagrange multiplier which takes into account the normalization condition. Equation (4.16) leads to the integral equation

$$\bar{\alpha}(x)=\frac{\exp\left[-\rho\beta\int_{-1}^{1}dx'\bar{\alpha}(x')K(x,x')\right]}{\int_{-1}^{1}dx\exp\left[-\rho\beta\int_{-1}^{1}dx'\bar{\alpha}(x')K(x,x')\right]}\ . \tag{4.18}$$

Note that the isotropic configuration $\bar{\alpha}\equiv\frac{1}{2}$ always solves Eq. (4.18) because

$$\int_{-1}^{1}dx'K(x,x')=u_0 \tag{4.19}$$

is independent of x [see Eq. (4.2)].

The actual structure of the kernel $K(x,x')$ [Eq. (4.2)] implies the following form for $\bar{\alpha}(x)$:

$$\bar{\alpha}(x)=C\exp\left[-\rho\beta\sum_{l=1}^{\infty}(2l+1)u_l\alpha_lP_l(x)\right]$$
$$=C\exp[\gamma_1x+\gamma_2P_2(x)+\gamma_3P_3(x)+\cdots] \tag{4.20}$$

with

$$\frac{1}{C}=\int_{-1}^{1}dx\exp\left[\sum_{l=1}^{\infty}\gamma_lP_l(x)\right]\ . \tag{4.21}$$

One should recall that within our approximation $\gamma_l=0$ for $l\geq5$ because we consider only terms up to $O(m^8)$. If we insisted on a strict expansion of $\bar{\alpha}(x)$ in powers of m^2, we would have to expand the exponential functions in Eqs. (4.20) and (4.21) too and truncate this series accordingly. However, we refrain from this systematic scheme in favor of keeping the full exponential form in Eq. (4.20), which differs from a simple polynomial expression for $\bar{\alpha}(x)$.

Equation (4.20) leads to a system of coupled nonlinear equations for the coefficients γ_l:

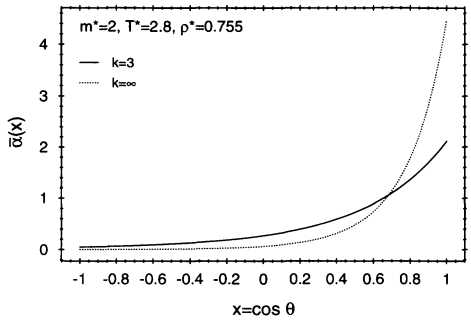

FIG. 4. Typical orientational distributions $\bar{\alpha}(\cos\theta)$ in the ferroelectric phase for aspect ratios $k=3$ and ∞. They exhibit a pronounced maximum at $\cos\theta=1$, i.e., in the direction of the long axis of the ellipsoidal sample. But even for the needle-shaped sample there is still a finite probability for the dipole moment to point into other directions (cf. Sec. VIII).

$$\gamma_l=-\rho\beta\frac{(2l+1)^2}{2}u_l\int_{-1}^{1}dx\,P_l(x)\exp\left[\sum_{i=1}^{\infty}\gamma_iP_i(x)\right]$$
$$\times\left[\int_{-1}^{1}dx'\exp\left[\sum_{j=1}^{\infty}\gamma_jP_j(x')\right]\right]^{-1},\ j\geq1\ . \tag{4.22}$$

The coefficients α_l, which determine $\bar{\alpha}(x)$, follow from

$$\alpha_l=-\frac{\gamma_l}{\rho\beta(2l+1)u_l} \tag{4.23}$$

for $l=1,\ldots,p$ if the u_l are expanded up to $O(m^{2p})$. Based on Eqs. (4.9)–(4.12), the above nonlinear system of equations is solved numerically by using a standard routine of the Numerical Algorithms Group library, which requires an initial guess as input and which finds the solution by iteration. Thereby it is convenient to describe Stockmayer fluids in terms of the reduced density $\rho^*=\rho\sigma^3$, the reduced temperature $T^*=k_BT/\epsilon$, the reduced dipole moment $m^*=(m^2/\epsilon\sigma^3)^{1/2}$, and the reduced chemical potential $\mu^*=[\mu-k_BT\ln(6\lambda^3/\pi d^3)]/\epsilon$. A typical solution of Eqs. (4.15) and (4.22) together with Eqs. (4.20), (4.21), and (4.23), exhibiting the expected pronounced maximum at $x=1$, is shown in Fig. 4, where $m^*=2$, $T^*=2.8$, $k=3$, and $\mu^*=-4.677$, giving $\rho^*=0.755$. Since $K(-x,-x')=K(x,x')$ the function $\bar{\alpha}(-x)$ is a solution as well, representing a fluid polarized along the opposite direction.

V. PHASE DIAGRAMS

The conditions for coexistence of a ferroelectrically ordered phase of density ρ_f and an isotropic phase of density ρ_i along the phase boundary $\mu_f(T)$ are

$$\Omega[\rho_i,\{\bar{\alpha}\equiv\tfrac{1}{2}\},T,\mu_f]=\Omega[\rho_f,\{\bar{\alpha}(x)\},T,\mu_f] \tag{5.1}$$

and

$$\left.\frac{\partial\Omega}{\partial\rho}\right|_{\rho_i,\bar{\alpha}\equiv/2}=0\ ,$$
$$\left.\frac{\partial\Omega}{\partial\rho}\right|_{\rho_f,\{\bar{\alpha}(x)\}}=0\ , \tag{5.2}$$
$$\left.\frac{\delta\Omega}{\delta\bar{\alpha}}\right|_{\rho_f,\{\bar{\alpha}(x)\}}=0\ .$$

Since $\Omega[\rho,\{\bar{\alpha}(x)\},T,\mu]=F[\rho,\{\bar{\alpha}(x)\},T]-\mu\rho V$ the chemical potential μ_f can be eliminated from these equations, resulting in the following equations for the unknowns ρ_i, ρ_f, and $\{\alpha_l, l\geq 1\}$:

$$f_{\rm ref}^{\rm HS}(\rho_i)-\rho_i\mu_{\rm HS}(\rho_i)-\tfrac{1}{4}\rho_i^2u_0 = f_{\rm ref}^{\rm HS}(\rho_f)-\rho_f\mu_{\rm HS}(\rho_f)-\rho_f^2\sum_{l=0}^{p}u_l\alpha_l^2\ , \tag{5.3}$$

$$\mu_{\rm HS}(\rho_i)+\tfrac{1}{2}\rho_iu_0=\mu_{\rm HS}(\rho_f)+\frac{1}{\beta}\left[\ln(2C)+\sum_{l=1}^{p}\frac{2}{2l+1}\alpha_l\gamma_l\right] +2\rho_f\sum_{l=0}^{p}u_l\alpha_l^2\ , \tag{5.4}$$

and Eq. (4.22) with $\rho=\rho_f$. By using Eq. (4.23), Eqs. (5.4) and (4.22) can be rewritten as

$$\mu_{\rm HS}(\rho_i)+\tfrac{1}{2}\rho_iu_0=\mu_{\rm HS}(\rho_f)+\tfrac{1}{2}\rho_fu_0+\frac{1}{\beta}\left[\ln 2-\ln\int_{-1}^{1}dx\,\exp\left[-\rho_f\beta\sum_{l=1}^{p}(2l+1)u_l\alpha_lP_l(x)\right]\right] \tag{5.5}$$

and

$$\alpha_l=\frac{2l+1}{2}\frac{\int_{-1}^{1}dx\,P_l(x)\exp\left[-\rho_f\beta\sum_{i=1}^{p}(2i+1)u_i\alpha_iP_i(x)\right]}{\int_{-1}^{1}dx\,\exp\left[-\rho_f\beta\sum_{i=1}^{p}(2i+1)u_i\alpha_iP_i(x)\right]}\ . \tag{5.6}$$

The coexistence line between the ferroelectrically ordered phase and the isotropic phase is given by

$$\mu_f(T)=\mu_{\rm HS}[\rho_i(T),T]+\tfrac{1}{2}\rho_i(T)u_0\ . \tag{5.7}$$

Due to $\Omega=-pV$ the corresponding pressure at coexistence is

$$p_f(T)=-f_{\rm ref}^{\rm HS}[\rho_i(T)]-\tfrac{1}{4}\rho_i^2u_0+\mu_f(T)\rho_i(T)\ . \tag{5.8}$$

Figure 5 shows the phase diagram for $m^*=2$ and $k=3$. At low temperatures ($T<T_3$) a ferroelectric liquid coexists with an isotropic gas. The dotted curves indicate the liquid-gas phase diagram if no ordered phases are taken into account (i.e., α_l is constrained to be zero for $l\geq 1$). At the triple point temperature $T_3^*=2.494$ three phases coexist: the isotropic gas, an isotropic liquid, and a ferroelectric liquid. Up to $T^*=T_c^*=2.552$ coexistence of both isotropic phases or both liquid phases is possible. Above T_c there is only one isotropic phase left. The density difference between the coexisting unordered and ordered fluids shrinks to zero at the tricritical point T_t with $T_t^*=2.727$. For temperatures above T_t there is a line of second-order phase transitions $\rho_{fc}(T)$ (dashed curve). The tricritical point exhibits the classical critical exponents as predicted by an extended Landau theory [34]:

$$\alpha_1\sim(T_t-T)^{1/2}\ ,\quad \rho_f-\rho_t\sim T_t-T\ ,\quad T\nearrow T_t \tag{5.9}$$

along two-phase coexistence $[\mu=\mu_f(T)]$ for $T<T_t$ and

$$\alpha_1\sim(\mu-\mu_t)^{1/4}\ ,\quad \rho(T_t,\mu)-\rho_t\sim(\mu-\mu_t)^{1/2}\ ,\quad \mu\searrow\mu_t \tag{5.10}$$

for fixed $T=T_t$, where $\rho_t=\rho(T_t,\mu_f(T_t))$ is the tricritical density. Up to logarithmic corrections, in three spatial dimensions these critical exponents are valid beyond mean field theory. α_1 plays the role of the order parameter since the coefficients $\alpha_{l\geq 2}$ vanish more rapidly (see

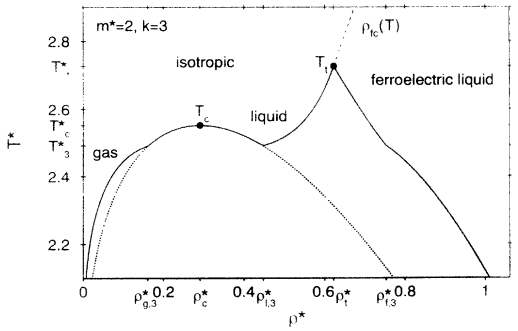

FIG. 5. Phase diagram for the dipole moment $m^*=2$ and the aspect ratio $k=3$. Below the triple temperature T_3 a ferroelectric liquid coexists with an isotropic gas. Between T_3 and the critical temperature T_c there are three possible phases: an isotropic gas, an isotropic liquid, and a ferroelectric liquid. The first-order phase transition between the isotropic and the ferroelectric liquid turns into a second-order phase transition at the tricritical temperature T_t. Above T_t there is a line of critical points $\rho_{fc}(T)$ given by the dashed curve. The dotted lines denote the two phase region of the isotropic gas and the liquid if the ferroelectric phase is not taken into account. Within the shaded region there are no thermodynamically stable states. At high densities the system freezes. The corresponding solid phase is not shown because it is not accessible by the present theory.

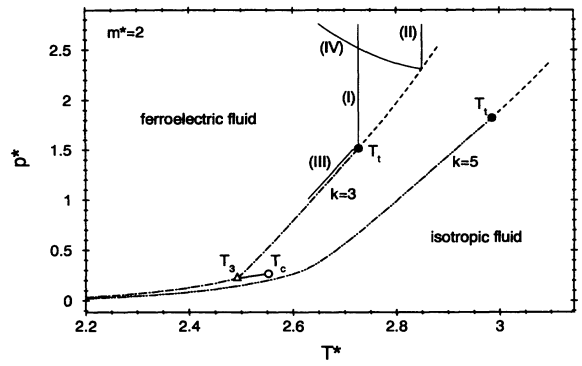

FIG. 6. Pressure-temperature phase diagrams for $m^*=2$ and $k=3$, 5. For $k=3$ the solid line denotes the coexistence line of the isotropic gas and liquid ending in a critical point T_c (open circle); the triple point T_3 is indicated by a triangle. For $k=5$ at all temperatures only two phases can coexist, an isotropic and a ferroelectric fluid (see also Fig. 9). The positions of the tricritical points are indicated by full circles. As before, the melting curves are missing. The behavior of the density and the orientational order along the thermodynamic paths (I)–(IV) is displayed in Figs. 7 and 8.

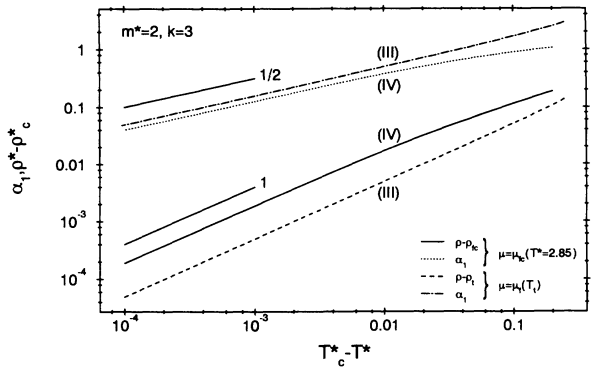

FIG. 8. Dependence of the ferroelectric order parameter α_1 and the density difference $\rho^*-\rho^*_{fc}$ on the temperature for a fixed chemical potential $\mu=\mu_{fc}(T^*=2.85)$ upon approaching the order-disorder transition above the tricritical point T_t along the thermodynamic path (IV) shown in Fig. 6 (dotted and solid line) and variation of α_1 and $\rho^*-\rho^*_t$ along the coexistence line $\mu_f(T)$ upon approaching T_t (dash-dotted and dashed lines); see the thermodynamic path (III) shown in Fig. 6. In the latter case the liquid density ρ corresponds to that of the ferroelectrically ordered phase. The slopes correspond to the critical exponents $\frac{1}{2}$ and 1 given by Eqs. (5.11) and (5.9).

Sec. VI). Upon approaching a point T_0 on the line of critical points $\rho_{fc}(T)$ *above* T_t one finds

$$\alpha_1\sim(T_0-T)^{1/2}\ ,\quad T\nearrow T_0\ ,\quad \mu \text{ fixed}$$
$$\rho-\rho_{fc}(T_0)\sim T-T_0\ ,\quad T\to T_0^{\pm}\ ,\quad \mu \text{ fixed} \tag{5.11}$$

and

$$\alpha_1\sim(\mu-\mu_{fc})^{1/2}\ ,\quad \mu\searrow\mu_{fc}(T)\ ,\quad T \text{ fixed}$$
$$\rho-\rho_{fc}(T)\sim\mu-\mu_{fc}(T)\ ,\quad \mu\to\mu_{fc}(T)^{\pm}\ ,\quad T \text{ fixed}\ . \tag{5.12}$$

These critical exponents are mean-field-like. By taking into account the critical fluctuations (which is beyond the scope of the present density-functional theory) the exponent for α_1 in Eqs. (5.11) and (5.12) is expected to be replaced by $\beta\approx 0.35$.

Figure 6 shows the phase diagram in the pressure-temperature plane using the reduced pressure $p^*=p\sigma^3/\epsilon$. The full variation of α_1 and ρ along the various thermodynamic paths described above is displayed in Figs. 7 and 8 for $m^*=2$ and $k=3$.

For larger aspect ratios k the liquid-gas critical point vanishes so that at all temperatures there are only two possible phases (see Fig. 9 with $k=5$; a similar topology of the phase diagram has been found in Refs. [35–37] for

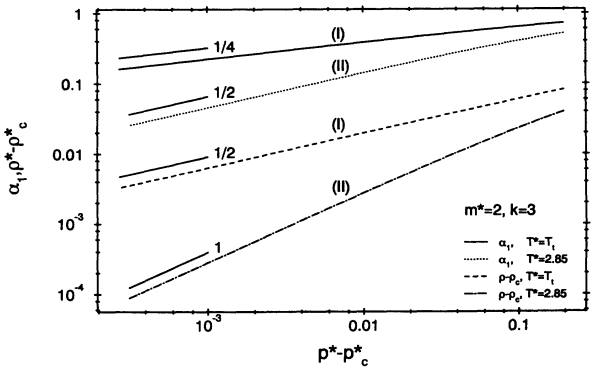

FIG. 7. Dependence of the ferroelectric order parameter α_1 and the density difference $\rho^*-\rho^*_c$ on the pressure difference $p^*-p^*_c$ along the isotherms $T^*=2.85$ (II) and $T^*=T^*_t=2.7266$ (I) shown in Fig. 6. The slopes in the double logarithmic plot correspond to the critical exponents 1, $\frac{1}{2}$, and $\frac{1}{4}$, respectively given by Eqs. (5.12) and (5.10).

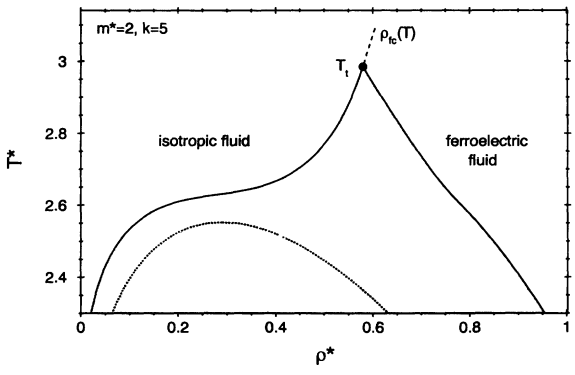

FIG. 9. Phase diagram for $m^*=2$ and $k=5$ exhibiting only two phases, an anisotropic fluid at low densities and a ferroelectric fluid at high densities. The dashed line $\rho_{fc}(T)$ indicates the line of second-order phase transitions above the tricritical temperature T_t. As in Fig. 5 the dotted curve is the phase diagram if the ferroelectric phase is not taken into account. Within the shaded region there are no thermodynamically stable states. Note that in comparison to Fig. 5 the critical point T_c has disappeared. The solid phase is missing.

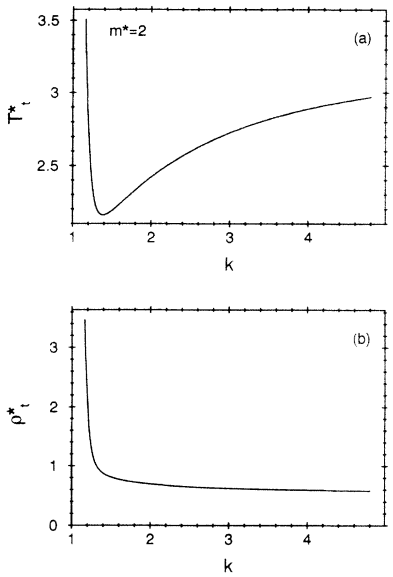

FIG. 10. Dependence of (a) the tricritical temperature T_t^* and (b) the tricritical density ρ_t^* on the aspect ratio k for $m^*=2$. At large aspect ratios T_t^* approaches the limiting value $T_t^*(k\to\infty)=3.2595$ and $\rho_t^*(k\to\infty)=0.5433$. For small k, T_t^* increases sharply. However, for these small values of k the corresponding tricritical density reaches such high values that the fluid will become a solid.

three- and two-dimensional fluids with internal quantum states). For decreasing k the tricritical point first approaches the triple point, but then the tricritical temperature increases again (see Fig. 10). As shown in Fig. 11 for the case of a sphere, at small values of k there is only a weakly first-order transition between the isotropic and the ferroelectric liquid below the tricritical point, which occurs at a density far above solidification. Of course these phase diagrams are incomplete insofar as they do

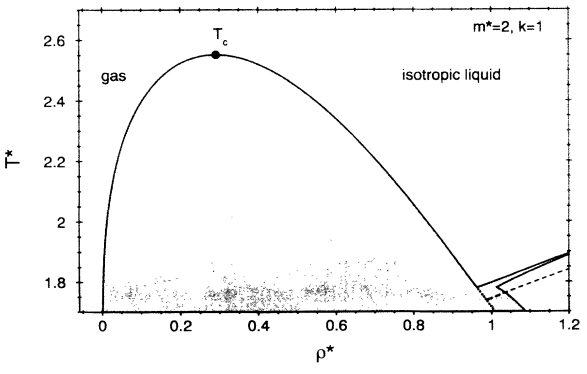

FIG. 11. Phase diagram for a spherical sample ($k=1$). The formation of a ferroelectric phase affects the phase diagram only at very high densities where a weakly first-order transition between the isotropic and ferroelectric liquid is found, which extends up to the highest densities considered. The dashed line denotes the absolute stability limit of the isotropic phase given by Eq. (7.10), which represents the analytic continuation of $\rho_{fc}(T)$ (compare Figs. 5 and 9).

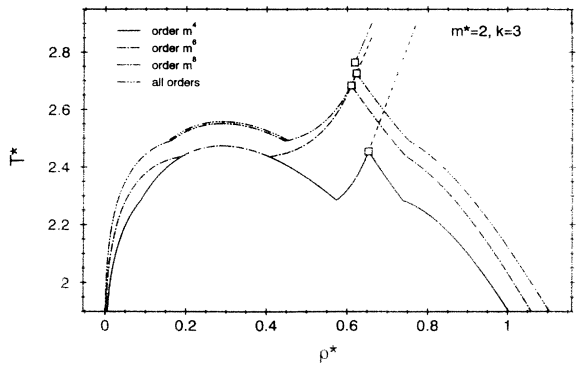

FIG. 12. Comparison of the phase diagrams for $m^*=2$ and $k=3$ obtained by approximating the coefficients u_l in different orders in m [see Eq. (4.5)]. Since the isotropic-liquid–gas part of the phase diagram depends only on u_0, it is the same in $O(m^4)$ and $O(m^6)$ [see Eq. (4.9)]. The line of critical points (dashed line) depends only on u_1 [see Eq. (7.10)]. Therefore it is the same in $O(m^6)$ and $O(m^8)$ [Eq. (4.10)]. Also shown are those parts of the limiting phase diagram that can be calculated to *all* orders in m, i.e., the line of critical points, the tricritical point (open squares), and the isotropic-liquid–gas coexistence line.

not contain the transition to a solid phase which is not predicted by the present local density-functional theory. For a pure Lennard-Jones fluid the liquid-solid transition occurs in the range $\rho^*=0.85$–0.95 for $T<T_c$ [24], so that most probable for values of k close to 1 the formation of the ferroelectric phase is preempted by the freezing of the fluid.

All results presented up to now were obtained with the coefficients u_l calculated in order m^8 [see Eqs. (4.9)–(4.13)]. The effect of truncating the series in Eq. (4.4) can be estimated from Fig. 12, which displays the phase diagrams obtained with truncations at $O(m^4)$, $O(m^6)$, and $O(m^8)$ for $k=3$ and $m^*=2$. Additionally we show parts of the phase diagram using the full exponential $\exp(\beta w_{\rm dip})$, i.e., *all* orders in m: The coexistence line of the isotropic fluids is taken from Ref. [18]; the tricritical point and the line of critical points are calculated from Eqs. (7.10) and (7.24) (using the results for $\hat{f}_{110}$ and $\hat{f}_{220}$ from Ref. [18] to determine u_1 and u_2). Note that the liquid-gas coexistence line is the same for $O(m^4)$ and $O(m^6)$ because it depends only on u_0, which contains only even powers of m^2 [see Eq. (4.9)]. On the other hand, the line of critical points is identical for $O(m^6)$ and $O(m^8)$ since u_1 contains only odd powers of m^2. Obviously with increasing order in m the phase diagrams converge to a limiting form for which the result in $O(m^8)$ represents a satisfying approximation.

VI. OBLATE SAMPLES

In the case of oblate ellipsoidal samples, i.e., at aspect ratios $k<1$, the polarization is expected to point along a spontaneously chosen direction within the xy plane. This means that the orientational distribution $\alpha(\omega)$ will depend also on the azimuthal angle ϕ. Thus we use an ex-

pansion in spherical harmonics:

$$\alpha(\omega)=\sum_{l,m}\mu_{lm}Y_{lm}(\omega)\ ,\quad \mu_{lm}=\int d\omega\,\alpha(\omega)Y^*_{lm}(\omega)\ . \tag{6.1}$$

$$\frac{1}{V}\Omega_{\rm int}=-\frac{\rho^2}{2\beta}\sum_{l_1,l_2,l}\int_{2V\setminus S_\sigma}d^3r_{12}h\left[\theta_{12},\frac{r_{12}}{2R}\right]\hat{f}_{l_1l_2l}(r_{12})$$
$$\times\int d\omega\,d\omega'\sum_{m_1,m_2,m}\mu^*_{l_1m_1}\mu^*_{l_2m_2}Y^*_{l_1m_1}(\omega)Y^*_{l_2m_2}(\omega')C(l_1l_2l,m_1m_2m)$$
$$\times Y_{l_1m_1}(\omega)Y_{l_2m_2}(\omega')Y^*_{lm}(\omega_{12})\ , \tag{6.2}$$

where the complex conjugate of Eq. (6.1) has been used. Only the factor $Y^*_{lm}(\omega_{12})$ depends on the angle ϕ_{12}, so that all terms with $m\neq 0$ vanish. By using the orthogonality of the spherical harmonics and with $Y_{l0}(\omega)=\sqrt{(2l+1)/4\pi}P_l(\cos\theta)$ one obtains

$$\frac{1}{V}\Omega_{\rm int}=-2\pi\frac{\rho^2}{2\beta}\sum_{l_1,l_2,l}\left[\frac{2l+1}{4\pi}\right]^{1/2}\sum_m C(l_1l_2l,m\bar{m}0)$$
$$\times\mu^*_{l_1m}\mu^*_{l_2\bar{m}}I_{l_1l_2l}\ . \tag{6.3}$$

In the next step we use our results for the integrals I_Λ obtained in Sec. III. For $\Lambda=(ll0)$ we find [see Eq. (A.157) in Ref. [29]]

$$\sum_m C(ll0,m\bar{m}0)\mu^*_{lm}\mu^*_{l\bar{m}}=(2l+1)^{-1/2}(-1)^l\sum_m|\mu_{lm}|^2\ , \tag{6.4}$$

while for $\Lambda=(112)$ the explicit evaluation of the Clebsch-Gordan coefficients results in

$$\sum_m C(112,m\bar{m}0)\mu^*_{1m}\mu^*_{1\bar{m}}=\sqrt{\tfrac{2}{3}}(\mu_{10}^2-|\mu_{11}|^2)\ . \tag{6.5}$$

(Note that μ_{l0} is real.) By inserting Eqs. (3.18), (3.20), (6.4), and (6.5) into Eq. (6.3) the interaction contribution takes on the form

$$\lim_{V\to\infty}\frac{1}{V}\Omega_{\rm int}=\pi\rho^2\sum_{l,m}(2l+1)\hat{u}_l|\mu_{lm}|^2$$
$$-\frac{8\pi^2}{3}m^2\rho^2I(k)(\mu_{10}^2-|\mu_{11}|^2)\ , \tag{6.6}$$

where $\hat{u}_{l\neq 1}=u_l$ and $\hat{u}_1=1/(\beta\sqrt{\pi}3^{3/2})\int_\sigma^\infty dr\,r^2\hat{f}_{110}(r)$ is the shape independent part of u_1. In order to obtain a convenient notation we rewrite this as

$$\lim_{V\to\infty}\frac{1}{V}\Omega_{\rm int}=\pi\rho^2\sum_{l,m}(2l+1)v_{lm}|\mu_{lm}|^2 \tag{6.7}$$

with $v_{lm}=u_l$ for $l\neq 1$, $v_{10}=\hat{u}_1-(8\pi/9)m^2I(k)$, and $v_{1\pm1}=\hat{u}_1+(4\pi/9)m^2I(k)$.

The minimization of the grand-canonical functional with respect to the orientational distribution yields

Since $\alpha(\omega)$ is real one has $\mu_{l\bar{m}}=(-1)^m\mu^*_{lm}$, where $\bar{m}\equiv -m$; $\mu_{00}=1/\sqrt{4\pi}$ due to Eq. (2.1). In analogy with Eq. (3.6) we obtain

$$\alpha(\omega)=C\exp\left[-2\pi\rho\beta\sum_{l,m}(2l+1)v_{lm}\mathrm{Re}(\mu_{lm}Y_{lm}(\omega))\right]\ . \tag{6.8}$$

Here we used $[\delta/\delta\alpha(\omega)]|\mu_{lm}|^2=2\,\mathrm{Re}(\mu_{lm}Y_{lm}(\omega))$. From Eq. (6.8) one obtains a system of equations for C and the unknown expansion coefficients μ_{lm} of the orientational distribution:

$$\mu_{lm}=C\int d\omega\,Y^*_{lm}(\omega)\exp\left[-2\pi\rho\beta\sum_{l,m}(2l+1)v_{lm}\right.$$
$$\left.\times\mathrm{Re}(\mu_{lm}Y_{lm}(\omega))\right]\ , \tag{6.9}$$
$$C^{-1}=\int d\omega\exp\left[-2\pi\rho\beta\sum_{l,m}(2l+1)v_{lm}\right.$$
$$\left.\times\mathrm{Re}(\mu_{lm}Y_{lm}(\omega))\right]\ .$$

As in Eqs. (4.20) and (4.21) the sum in the exponent contains only a finite number of terms if the coefficients v_{lm} are expanded with respect to the dipole moment m and then truncated at a certain order.

In order to examine the resulting orientational distribution it is useful to perform a transformation to a different coordinate system whose z' axis points into the spontaneously chosen direction of the polarization which lies within the xy plane (see Sec. III). For a general rotation described by the Euler angles $\Omega=(\phi,\theta,\chi)$ the spherical harmonics transform according to [29]

$$Y_{lm}(\omega')=\sum_n D^l_{nm}(\Omega)Y_{ln}(\omega)\ , \tag{6.10}$$

where $D^l_{nm}(\Omega)$ denotes a rotation matrix with

$$D^l_{nm}(\omega)=e^{-in\phi}d^l_{nm}(\theta)e^{-im\chi}\ . \tag{6.11}$$

A general expression as well as explicit formulas for $l=1$ and 2 for the functions d^l_{nm} are given in Ref. [29]. The coefficients of the orientational distribution corresponding to the new coordinate system are related to the previous ones according to

$$\mu'_{lm}=\sum_n[D^l_{nm}(\Omega)]^*\mu_{ln}\ . \tag{6.12}$$

Due to $\sum_m (D^l_{nm})^* D^l_{n'm} = \delta_{nn'}$, one has $\sum_m |\mu'_{lm}|^2 = \sum_m |\mu_{lm}|^2$, i.e., the shape independent part of $\Omega_{\rm int}$ [see Eq. (6.6)] takes on the same form in the new coordinates. Now we consider the special rotation $\phi=0$, $\theta=\pi/2$, and $\chi=\pi/2$, which represents the transformation $(x',y',z')=(y,z,x)$. Using the explicit expressions for the d^l_{nm} from Ref. [29] we find

$$\mu'_{10} = -\sqrt{2}\,\mathrm{Re}\mu_{11}\ , \quad \mu'_{11} = \mathrm{Im}\mu_{11} - \frac{i}{\sqrt{2}}\mu_{10}\ . \tag{6.13}$$

Inserting Eq. (6.13) into Eq. (6.6) yields the interaction contribution in the new coordinates

$$\begin{aligned}\lim_{V\to\infty}\frac{1}{V}\Omega_{\rm int} = &-\frac{8\pi^2}{3}m^2\rho^2 I(k)\\ &\times[2(\mathrm{Im}\mu'_{11})^2-(\mathrm{Re}\mu'_{11})^2-\tfrac{1}{2}\mu_{10}'^2]\\ &+\pi\rho^2\sum_{l,m}(2l+1)\hat{u}_l|\mu'_{lm}|^2\ .\end{aligned} \tag{6.14}$$

In the following we exploit the symmetries expected for the equilibrium distribution in order to reduce the number of coefficients that have to be determined. Due to the invariance of Ω under rotations of $\alpha(\omega)$ about the z axis one can choose the polarization to point along the z' axis, which results in $\mu'_{11}=0$. Any other degenerate solution of Eq. (6.9) can then be obtained by rotating the previous solution about the z axis by an angle ϕ_0. Furthermore the orientational distribution should be invariant under a reflection at the $x'z'$ plane, i.e., the middle plane of the ellipsoid. This means that it has to be an even function of the angle ϕ'. For this reason the imaginary parts of the coefficients μ'_{lm} vanish since $\mathrm{Im}Y_{lm}(\theta,\phi) = -\mathrm{Im}Y_{lm}(\theta,-\phi)$. Another symmetry operation is the reflection at the $y'z'$ plane corresponding to the transformation $\phi'\to\pi-\phi'$. Due to $Y_{lm}(\theta,\pi-\phi)=(-1)^m Y^*_{lm}(\theta,\phi)$ all coefficients μ'_{lm} with even m are real, while coefficients with odd m are imaginary and thus must be zero. For example, for $l\le 2$ one is left only with the real coefficients μ'_{10}, μ'_{20}, and μ'_{22}.

Surprisingly the numerical solutions of Eq. (6.9) show that at the minimum of the grand-canonical functional, μ'_{22} as well as the higher coefficients with $m\neq 0$ vanish. This means that the orientational distribution exhibits rotational symmetry about the z' axis and thus depends only on the angle θ'. With the definition

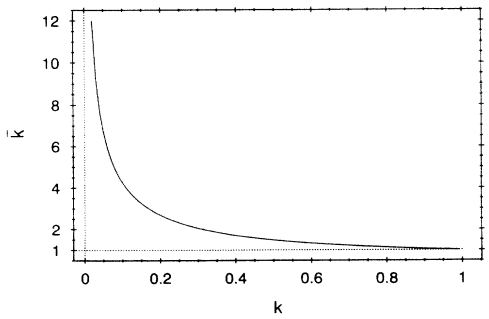

FIG. 13. The phase behavior and the structural properties of oblate samples with an aspect ratio $k<1$ are equivalent to those of a certain elongated sample with an aspect ratio $\bar{k}>1$ [see Eq. (6.16)]. $\bar{k}=1$ for $k=1$ and $\bar{k}$ diverges for $k\to 0$.

$$\tilde{\alpha}_l = \frac{2l+1}{2}\int d\omega'\alpha(\omega')P_l(\cos\theta') = \sqrt{\pi(2l+1)}\,\mu'_{l0} \tag{6.15}$$

the grand-canonical potential Eq. (6.14) takes on exactly the same form as for elongated samples, but with α_l and $I(k)$ replaced by $\tilde{\alpha}_l$ and $-\frac{1}{2}I(k)$, respectively [see Eqs. (3.22)–(3.24) and recall that $\hat{u}_{l\neq 1}=u_l$]. Therefore the case of an oblate ellipsoid with aspect ratio k can be mapped onto the case of an elongated ellipsoid with an aspect ratio $\bar{k}$ given by the implicit equation

$$I(k) = -2I(\bar{k}) \tag{6.16}$$

whose solution is shown in Fig. 13. The aspect ratio $\bar{k}$ increases from 1 at $k=1$ to infinity at $k=0$. Not only are the phase diagrams identical for the aspect ratios k and $\bar{k}$, but also the orientational distributions at a given density and temperature are the same, except that they are centered around the z axis for $\bar{k}>1$ and around the z' axis for $k<1$.

VII. LANDAU THEORY

In order to locate the line of critical points separating the isotropic and ferroelectric liquid and to analyze the behavior near those second-order phase transitions we expand the orientation dependent contribution $\Delta\Omega$ to the grand-canonical potential [see Eq. (4.17)] for small deviations from isotropy, i.e., for small α_l. The corresponding entropic term is given by

$$\begin{aligned}&\int_{-1}^{1} dx\ \bar{\alpha}(x)\ln[2\bar{\alpha}(x)]\\ &\quad=\int_{-1}^{1} dx\left[\tfrac{1}{2}+\sum_{l=1}^{\infty}\alpha_l P_l(x)\right]\ln\left[1+2\sum_{l=1}^{\infty}\alpha_l P_l(x)\right]\\ &\quad=\sum_{n=2}^{\infty}(-1)^n\frac{2^{n-1}}{n(n-1)}\int_{-1}^{1}dx\left[\sum_{l=1}^{\infty}\alpha_l P_l(x)\right]^n\ .\end{aligned} \tag{7.1}$$

The multinomial expression in the integral can be expanded as

$$\begin{aligned}&\left[\sum_{l=1}^{\infty}\alpha_l P_l(x)\right]^n\\ &\quad=\lim_{N\to\infty}\sum_{k_1=0}^{n}\cdots\sum_{k_N=0}^{n}\delta_{k_1+\cdots+k_N,n}\begin{pmatrix} n\\ k_1,k_2,\ldots,k_N\end{pmatrix}\\ &\qquad\times[\alpha_1 P_1(x)]^{k_1}\cdots[\alpha_N P_N(x)]^{k_N}\end{aligned} \tag{7.2}$$

with the multinomial coefficients

$$\begin{pmatrix} n\\ k_1,k_2,\ldots,k_N\end{pmatrix} = \frac{n!}{k_1!k_2!\cdots k_N!}\ .$$

The terms of this sum can be ordered according to the index of the highest nonzero k_i, i.e., the degree r of the highest occurring Legendre polynomial. [For a given N-tuple $(k_1,\ldots,k_N)$, r is defined by $k_r\neq 0$ and $k_{i>r}=0$.] For that purpose we introduce the abbreviation

$$\begin{aligned}f(k_1,\ldots,k_N;n) = &\,\delta_{k_1+\cdots+k_N,n}\begin{pmatrix} n\\ k_1,k_2,\ldots,k_N\end{pmatrix}\\ &\times[\alpha_1 P_1(x)]^{k_1}\cdots[\alpha_N P_N(x)]^{k_N}\end{aligned} \tag{7.3}$$

and rewrite Eq. (7.2) as

$$\left[\sum_{l=1}^{\infty}\alpha_l P_l(x)\right]^n=\lim_{N\to\infty}\left[\sum_{k_1=0}^{n}\cdots\sum_{k_{N-1}=0}^{n}f(k_1,\ldots,k_{N-1},k_N=0;n)+\sum_{k_1=0}^{n}\cdots\sum_{k_{N-1}=0}^{n}\sum_{k_N=1}^{n}f(k_1,\ldots,k_N;n)\right]. \tag{7.4}$$

The iteration of this procedure leads to

$$\left[\sum_{l=1}^{\infty}\alpha_l P_l(x)\right]^n=\lim_{N\to\infty}\sum_{r=1}^{N}\sum_{k_1=0}^{n}\cdots\sum_{k_{r-1}=0}^{n}\sum_{k_r=1}^{n}f(k_1,\ldots,k_r,k_{r+1}=0,\ldots,k_N=0;n)\,. \tag{7.5}$$

Thus the orientation dependent contribution to the grand-canonical potential is

$$\frac{1}{V}\Delta\Omega=\rho^2\sum_{l=1}^{\infty}u_l\alpha_l^2+\frac{\rho}{\beta}\sum_{n=2}^{\infty}\left[\sum_{r=1}^{\infty}\sum_{k_1=0}^{n}\cdots\sum_{k_{r-1}=0}^{n}\sum_{k_r=1}^{n}c_{k_1\cdots k_r}^{(r,n)}\alpha_1^{k_1}\cdots\alpha_r^{k_r}\right] \tag{7.6}$$

with

$$c_{k_1\cdots k_r}^{(r,n)}=\delta_{k_1+\cdots+k_r,n}(-1)^n\frac{2^{n-1}}{n(n-1)}\times\begin{pmatrix}n\\k_1,k_2,\ldots,k_r\end{pmatrix}\int_{-1}^{1}dx\,P_1^{k_1}(x)\cdots P_r^{k_r}(x)\,. \tag{7.7}$$

In Eq. (7.6) the contribution for $n=2$ gives

$$\frac{1}{V}\Delta\Omega=\frac{\rho}{\beta}\sum_{l=1}^{\infty}\left[\frac{2}{2l+1}+\rho\beta u_l\right]\alpha_l^2+\cdots\,, \tag{7.8}$$

where the ellipsis denotes all higher-order terms; they contain products of at least three factors α_l. The terms of the form $\alpha_i\alpha_j$ with $i\neq j$ vanish due to the orthogonality of the Legendre polynomials appearing in Eq. (7.7). Obviously, for given β and ρ the isotropic configuration $\{\alpha_{l\geq1}=0\}$ minimizes the grand-canonical functional if the conditions

$$\frac{2}{2l+1}+\rho\beta u_l\geq0\,,\quad l\geq1 \tag{7.9}$$

are fulfilled. The numerical evaluation of Eqs. (4.10)–(4.13) shows that Eq. (7.9) is fulfilled for $l=2,3,4$ and for all reasonable values of the parameters T, ρ, m, σ, ϵ, and k. But for $l=1$, since u_1 may take on quite large negative values, especially if $k\gg1$, there is a threshold density

$$\rho_{fc}(T)=-\frac{2/3}{\beta u_1(k,m,T)} \tag{7.10}$$

above which a stable isotropic phase cannot exist. The line $\rho=\rho_{fc}(T)$ is a line of second-order phase transitions as long as the density ρ at the global minimum of Ω is a continuous function of μ, as it is the case for $T>T_t$. This means that in this parameter region the criterion for the minimum of Ω with respect to $\{\alpha_l\}$ is indeed determined *only* by the terms *quadratic* in α_l [see Eq. (7.8)]. The equilibrium values of the coefficients α_l at this minimum are determined by the coupled equations $\partial\Delta\Omega/\partial\alpha_l=0$, $l\geq1$. In the ordered phase α_l^{eq} is nonzero and vanishes continuously upon approaching $\rho_{fc}(T)$.

In order to obtain the values of α_l^{eq} one needs to know the higher-order terms in Eq. (7.8) beyond the quadratic contribution. *A posteriori* it will turn out that the coefficients α_l^{eq} will vanish more rapidly upon approaching the phase transition the larger l is. This means that high powers of α_l^{eq} with large l can be of the same order of magnitude as small powers of α_l^{eq} with small l. Inspired by the actual solution [cf. Eq. (7.16)] it turns out that in order to determine α_l^{eq} it is appropriate to order Eq. (7.6) not according to the number $n=\sum_{i=1}^{r}k_i$ of the factors α_l (as it is necessary for the stability criterion [see Eq. (7.9)]), but according to the number $L=\sum_{i=1}^{r}ik_i$. This is accomplished by introducing in Eq. (7.6) an additional summation at the expense of a corresponding Kronecker delta symbol followed by an interchange of the order of the summations:

$$\frac{1}{V}\Delta\Omega=\rho^2\sum_{l=1}^{\infty}u_l\alpha_l^2+\frac{\rho}{\beta}\sum_{L=1}^{\infty}\left\{\sum_{n=2}^{\infty}\sum_{r=1}^{\infty}\sum_{k_1=0}^{n}\cdots\sum_{k_{r-1}=0}^{n}\sum_{k_r=1}^{n}\delta_{k_1+2k_2+\cdots+rk_r,L}c_{k_1\cdots k_r}^{(r,n)}\alpha_1^{k_1}\cdots\alpha_r^{k_r}\right\}. \tag{7.11}$$

Due to $P_l(-x)=(-1)^lP_l(x)$ the product of polynomials on the right-hand side of Eq. (7.7) is an odd (even) function of x if n is odd (even) so that $c_{k_1\cdots k_r}^{(r,n)}=0$ for n odd. It is easy to show that, for a given set of numbers k_i, $n=\sum_{i=1}^{r}k_i$ and $L=\sum_{i=1}^{r}ik_i$ differ by an even integer so Eq. (7.11) contains only contributions with even L. The evaluation of the curly bracket in Eq. (7.11) for $L=2$ and 4 yields

$$\frac{1}{V}\Delta\Omega=\frac{\rho}{\beta}\left[\rho\beta\sum_{l=1}^{\infty}u_l\alpha_l^2+\tfrac{2}{3}\alpha_1^2+(\tfrac{2}{5}\alpha_2^2-\tfrac{8}{15}\alpha_1^2\alpha_2+\tfrac{4}{15}\alpha_1^4)+\cdots\right]. \tag{7.12}$$

If one splits off one of the k_r highest-order polynomials $P_r(x)$ in Eq. (7.7), its degree r must be less than or equal to the degree of the product of the remaining polynomials

$P_1^{k_1}(x)\cdots P_r^{k_r-1}(x)$,

$$r\le\sum_{i=1}^{r-1}ik_i+(k_r-1)r\Longleftrightarrow 2r\le\sum_{i=1}^{r}ik_i\Longleftrightarrow r\le\frac{L}{2}\ ; \quad (7.13)$$

otherwise the coefficient $c_{k_1\cdots k_r}^{(r,n)}$ would vanish due to the orthogonality of the Legendre polynomials because the product of the remaining polynomials could be expressed as a linear combination of Legendre polynomials with orders less than r. The minimization condition in Eq. (4.16) is equivalent to $\partial\Delta\Omega/\partial\alpha_l=0$ for all l, which results in

$$2\rho\beta u_l\alpha_l+\sum_{L=2}^{\infty}\sum_{r=l}^{L/2}\sum_{n=2}^{\infty}\sum_{k_1=0}^{n}\cdots\sum_{k_{r-1}=0}^{n}\sum_{k_r=1}^{n}\delta_{k_1+2k_2+\cdots+rk_r,L}c_{k_1\cdots k_r}^{(r,n)}\frac{k_l}{\alpha_l}\alpha_1^{k_1}\cdots\alpha_r^{k_r}=0\ . \quad (7.14)$$

Due to $2r\le L$ [see Eq. (7.13)] and $r\ge l$ [see Eq. (7.14)] one has

$$\sum_{i=1}^{r}ik_i-l\ge l\ . \quad (7.15)$$

(This inequality means that, if α_i is proportional to y^i, so that the product $\alpha_l^{-1}\alpha_1^{k_1}\cdots\alpha_r^{k_r}$ is proportional to y^{L-l}, this product vanishes for $y\to 0$ at least as y^l.) For $\rho\ge\rho_{fc}$ the set of equations given in Eq. (7.14) can be solved consistently with the ansatz

$$\alpha_l=A_l y^l+O(y^{l+2})\ , \quad (7.16)$$

where

$$y=\sqrt{-\tfrac{3}{2}\beta\rho u_1-1}=\sqrt{\rho/\rho_{fc}-1}\ . \quad (7.17)$$

By inserting this ansatz into Eq. (7.14) and using Eq. (7.12) one obtains

$$-\tfrac{4}{3}y^2A_1y-\tfrac{16}{15}A_1A_2y^3+\tfrac{16}{15}A_1^3y^3+O(y^5)=0\ ,\quad l=1 \quad (7.18)$$

$$-\frac{4}{3}\frac{u_2}{u_1}A_2y^2+\tfrac{4}{5}A_2y^2-\tfrac{8}{15}A_1^2y^2+O(y^4)=0\ ,\quad l=2 \quad (7.19)$$

$$-\frac{4}{3}\frac{u_l}{u_1}A_ly^l+g_l(A_1,\ldots,A_l)y^l+O(y^{l+2})=0\ ,\quad l\ge 3\ . \quad (7.20)$$

$g_l(A_1,\ldots,A_l)$ are functions which, in principle, can be determined by evaluating the appropriate expansion coefficients $c_{k_1\cdots k_r}^{(r,n)}$. They do not depend on the higher-order amplitudes $A_{i>l}$ since these always occur together with a power of y higher than y^l and thus are contained in the higher-order terms in Eq. (7.20). In Eq. (7.20) there are no terms of order y^{l-1} or lower due to the condition in Eq. (7.15). The nonzero solutions of Eqs. (7.18) and (7.19) are

$$A_1^2=\frac{5}{4}\frac{3u_1-5u_2}{u_1-5u_2}\ ,\quad A_2=\frac{5}{2}\frac{u_1}{u_1-5u_2}\ . \quad (7.21)$$

For $m^*=2$ and $k>1.15$ one finds $u_1<5u_2<0$ for all temperatures so that $A_2>0$ and A_1 is real. At lower values of k the above expansion becomes invalid if $u_1=5u_2$; in these cases, however, the orientational order affects the phase diagram only for densities for which the fluid is expected to be already solid (see Sec. V) so that we do not pursue that farther. The remaining amplitudes A_l can be determined iteratively by solving the equations for $l\ge 3$. There are two solutions for A_1 and for all A_l with odd l which differ only by sign. They correspond to the two possible orientations of the polarization vector along the long axis of the ellipsoid.

Equation (7.16) means that α_1 is a suitable order parameter vanishing as the square root of the density difference upon approaching the phase transition. Close to the phase transition the higher-order coefficients α_l are proportional to powers of α_1. Figure 14 shows the numerical results for the first three coefficients α_l as a function of the density difference for $m^*=2$, $k=3$, and $T^*=2.8$. The asymptotic behavior according to Eqs. (7.16) and (7.21) is indicated.

In order to analyze the dependence of the orientational order on the chemical potential near the line of critical points we insert the approximate solutions Eqs. (7.16) and (7.17) into the minimum condition Eq. (4.15) and expand with respect to y, which leads to

$$\left[\rho_{fc}\left[\frac{\partial^2}{\partial\rho^2}f_{\rm HS}(\rho_{fc},T)+\frac{1}{2}u_0\right]-\frac{2}{3}\frac{A_1^2}{\beta}\right]y^2+O(y^4)-\Delta\mu=0 \quad (7.22)$$

with $\Delta\mu=\mu-\mu_{fc}$ and

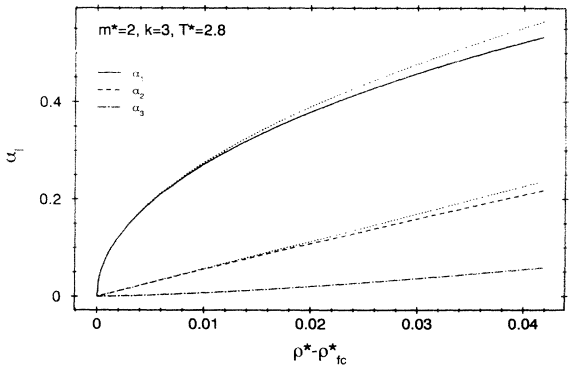

FIG. 14. Dependence of the expansion coefficients α_l of the orientational distribution on the density difference $\rho^*-\rho_{fc}^*$. In accordance with Eq. (7.16), α_l vanishes as $A_l\rho_{fc}^{*-l/2}(\rho-\rho_c)^{l/2}$ upon approaching the phase transition. The dotted lines represent the approximate solutions for α_1 and α_2 [Eq. (7.21)] obtained from the Landau expansion.

$$\mu_{fc}=\mu_{\rm HS}(\rho_{fc})+\tfrac{1}{2}\rho_{fc}u_0 \ . \tag{7.23}$$

For temperatures above T_t the coefficient of y^2 is positive. Thus there are solutions corresponding to the ordered phase for $\Delta\mu>0$, and since $y^2\sim\Delta\mu$ and $\alpha_1\sim y$, one obtains the critical exponents given in Eq. (5.12). At the tricritical point the expression in square brackets in Eq. (7.22) vanishes so that the terms of order y^4 become the leading ones and the critical exponents change to the values given in Eq. (5.10). By using Eq. (7.21) the implicit equation for the tricritical temperature reads

$$\frac{\partial^2}{\partial\rho^2}f_{\rm HS}[\rho_{fc}(T_t),T_t]+\tfrac{1}{2}u_0(T_t) = -\tfrac{5}{4}u_1(T_t)\frac{3u_1(T_t)-5u_2(T_t)}{u_1(T_t)-5u_2(T_t)} \ . \tag{7.24}$$

Note that T_t is independent of $u_{l\geq 3}$ [see Eq. (7.24)] and $\rho_{fc}(T)$ is independent of $u_{l\geq 2}$ [see Eq. (7.10)]. At lower temperatures, for which the prefactor of y^2 in Eq. (7.22) becomes negative, the solution of Eq. (7.22) corresponds to a saddle point of Ω, but there are minima at a larger degree of order which are not contained in the present expansion and which lead to the first-order transition.

VIII. DOMAIN FORMATION

As already stated above the present work is confined to the case of a homogeneous polarization throughout the sample. However, real ferromagnetic and ferroelectric samples with a finite demagnetization factor split up into various domains with different directions of the polarization vector in order to lower the demagnetization energy. For dipoles fixed on lattice sites Griffiths [38] has proven that this leads to a shape independent free energy in the thermodynamic limit. Provided that this result holds also for dipolar fluids, one can surmise [39] that the phase diagrams become independent of the sample shape if domain formation is taken into account. Since there is only one domain for an infinitely long needle-shaped sample ($k\to\infty$), or equivalently for a flat disk ($k\to 0$), our results for this special case would therefore be valid for any shape. For this reason in Fig. 15 we display the phase diagrams for $k\to\infty$ and for three different values of the dipole moment. For $m^*=2$ and 1.5 we find the same topological features as in Figs. 9 and 5. For $m^*=1$, however, the tricritical point has disappeared below the liquid-gas coexistence curve and only a critical end point $T_{\rm cep}$ is left where the line of critical points meets the coexistence line of the isotropic phases [40]. A similar series of phase diagrams has been found by Zhang and Widom [41], who use a phenomenological ansatz for the free energy. In contrast to their approach our analysis keeps track of the dependences on the microscopic parameters and renders, in addition, the orientational distribution $\bar{\alpha}(\cos\theta)$, which exhibits a nontrivial behavior even for $k=\infty$ (see Fig. 4).

Although for finite aspect ratios our results for a single domain probably do not correspond to the true thermodynamically stable configuration, they are nonetheless interesting on their own. First, they are indispensable prerequisites for the minimization of the density functional in a larger space of configurations including several domains. This allows one to determine the actual spatial distribution of the polarization in a ferroelectric dipolar fluid, which differs substantially from the case of a ferroelectric solid due to the lack of easy axes of the polarization. To our knowledge, up to now there are no microscopic results concerning this interesting but difficult problem, which we are pursuing actively. It has been surmised that the domain walls extend over the whole sample [42] whereas in snapshots of the configurations obtained by simulations the interface between domains with opposite polarization appears to be rather sharp [2]. One possible mechanism for reconciling these two observations would be that the sharp intrinsic interface migrates slowly throughout the system leading to an effective broadening over long times. Second, our results may be relevant for metastable states of homogeneous polarization, which could be observable in computer simulations using appropriate initial conditions.

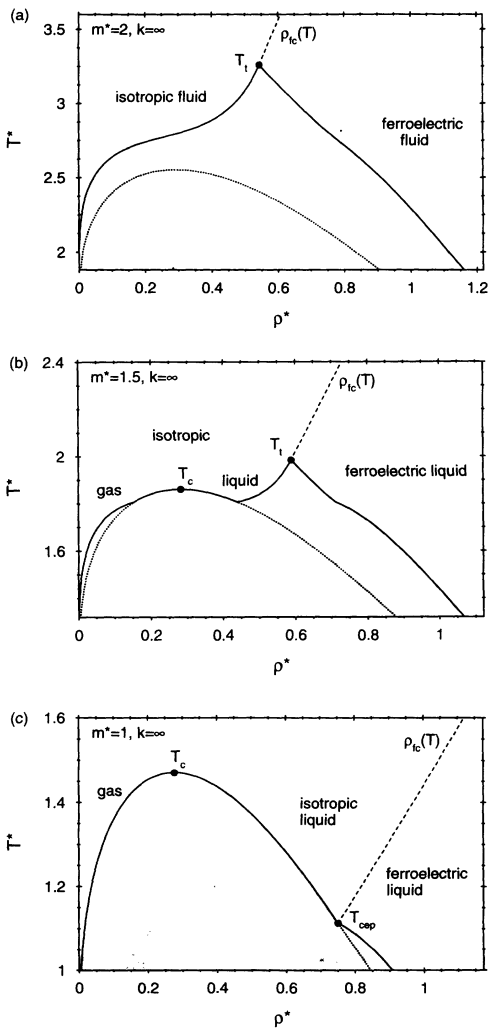

FIG. 15. Phase diagrams for needle-shaped samples ($k\to\infty$) with reduced dipole moments (a) $m^*=2$, (b) $m^*=1.5$, and (c) $m^*=1$. $T_{\rm cep}$ denotes a critical end point. For more details see the main text.

The shape dependence will certainly prevail if an external field is applied, which tends to suppress the domain formation. In a large field all dipoles are aligned in one direction and thus, e.g., the second virial coefficient becomes shape dependent [43] by the same mechanism as $\Omega_{\rm int}$ given in Eq. (2.10). Levy and Landau [30] showed experimentally that the specific heat at constant external field of a dipolar antiferromagnet depends on the aspect ratio of the sample. As compared to our shape dependent results in zero field the external field will shift the first-order phase transitions [41] and the line of second-order transitions will be washed out but leave fingerprints such as, e.g., maxima of the specific heat [40].

IX. SUMMARY

Based on the density-functional theory developed in Ref. [18] we have studied the occurrence and the properties of a ferroelectric nematic phase in Stockmayer fluids. The following main results have been obtained.

(i) For an ellipsoidal volume with a single domain, the shape dependence of the grand-canonical potential for ferroelectric phases, which is due to the long-range nature of the dipolar interaction, is given by Eqs. (3.22)–(3.24).

(ii) If the sample is surrounded by a dielectric continuum, the grand-canonical potential is given by Eq. (3.34). The introduction of a surrounding medium has the same effect on the free energy density as an increase of the aspect ratio k to $k_{\rm eff}(k,\epsilon)$ [see Eq. (3.35) and Fig. 3].

(iii) We have derived a scheme which allows us to determine the grand-canonical potential to any desired order in the dipole moment m (see Appendixes A and B). Explicit results up to $O(m^8)$ are given in Eqs. (4.9)–(4.13).

(iv) Figure 5 shows the phase diagram for $k=3$ exhibiting three fluid phases, a triple point, the usual liquid-gas critical point, a tricritical point, and a line of critical points corresponding to a second-order phase transition between the isotropic and the ferroelectric liquid.

(v) As shown in Fig. 9 for $k=5$, the liquid-gas critical point disappears for large aspect ratios so that in these systems at all temperatures there are only two fluid phases.

(vi) For nearly spherical samples, i.e., k close to 1, the occurrence of the ferroelectric phase affects the phase diagrams only at very high densities where the fluid is expected to have already turned into a solid (see Fig. 11).

(vii) The phase behavior and the structural properties of an oblate sample with an aspect ratio $k<1$ are equivalent to those of a certain elongated sample with an aspect ratio $\bar{k}>1$ (see Sec. VI and Fig. 13).

(viii) Close to the line of second-order phase transitions $\rho_{fc}(T)$ above the tricritical point the expansion coefficients α_l of the orientational distribution vanish according to the power law $\sim(\rho-\rho_{fc})^{l/2}$ [Eq. (7.16)]. The corresponding amplitudes for $l=1,2$, which are determined by a systematic Landau expansion, are compared with the full numerical results in Fig. 14.

(ix) Figures 7 and 8 show the critical exponents of the ferroelectric order parameter α_1 and the density difference $\rho-\rho_c$ upon approaching the phase transition at and above the tricritical point along various thermodynamic paths. They are in accordance with the systematic Landau theory [see Eqs. (5.9)–(5.12)].

(x) There are reasons to expect that for any shape of the sample the inclusion of domain formation leads to the phase diagrams obtained for $k=\infty$, which are displayed in Fig. 15 (see Sec. VIII).

Obviously several further investigations are lying ahead, such as the study of domain formation and the use of more sophisticated density-functional theories. In particular one would be interested in the freezing transition between the ferroelectric liquid and the solid phase as well as in more sophisticated expressions for the pair distribution function compared with the one used in Eq. (2.11).

ACKNOWLEDGMENTS

We would like to thank P. Frodl for helpful discussions as well as A. Haase and W. Koch for their assistance with computer programs.

APPENDIX A: DETERMINATION OF THE COEFFICIENTS u_l UP TO ORDER m^8

The contributions to u_l of order m^4 can be obtained from Eq. (4.3) if one replaces the Mayer function $\bar{f}$ by $\frac{1}{2}\beta^2 w_{\rm dip}^2 e^{-\beta w_{\rm LJ}}$. This yields [see Eq. (2.17)]

$$u_l^{(4)}=-\frac{256\pi^{7/2}}{15}\frac{(-1)^l}{(2l+1)^{3/2}}\frac{\beta}{\sigma^3}I_4(\beta\epsilon)\times\int d\omega\, d\omega' \Phi_{112}^2\Phi_{l10}^{*}\ . \tag{A1}$$

Φ_{112}^2 is expressed as a sum over rotational invariants using the product rule Eq. (B8), which is derived in Appendix B. Evaluation of the angular integrations with the help of the orthogonality relation Eq. (4.6) then gives $[\binom{220}{000}=1/\sqrt{5}]$

$$u_l^{(4)}=-24\pi\sqrt{5}\frac{(-1)^l}{(2l+1)^{1/2}}\frac{\beta}{\sigma^3}I_4(\beta\epsilon)\times\begin{pmatrix}1&1&l\\0&0&0\end{pmatrix}^2\begin{Bmatrix}1&1&2\\1&1&2\\l&l&0\end{Bmatrix} \tag{A2}$$

with the dimensionless integrals I_n defined in Eq. (4.14). Due to the triangle condition

$$|l_1-l_2|\le l\le l_1+l_2 \tag{A3}$$

for the $3j$ symbol $\binom{l_1\ l_2\ l}{m_1 m_2 m}$ and the parity selection rule

$$\begin{pmatrix}l_1&l_2&l\\0&0&0\end{pmatrix}=0 \quad \text{unless } l_1+l_2+l \text{ even} \tag{A4}$$

[see Eqs. (A.131) and (A.155) in Ref. [29]], $u_l^{(4)}$ is nonzero only for $l=0$ and 2:

$$u_0^{(4)}=-\frac{8\pi}{3}\frac{\beta}{\sigma^3}I_4(\beta\epsilon)\ ,\quad u_2^{(4)}=-\frac{8\pi}{375}\frac{\beta}{\sigma^3}I_4(\beta\epsilon)\ . \tag{A5}$$

Here the values

$$\begin{bmatrix}1&1&0\\0&0&0\end{bmatrix}=-\frac{1}{\sqrt{3}}\ ,\quad \begin{bmatrix}1&1&2\\0&0&0\end{bmatrix}=\sqrt{\tfrac{2}{15}} \tag{A6}$$

and

$$\begin{Bmatrix}1&1&2\\1&1&2\\0&0&0\end{Bmatrix}=\frac{1}{3\sqrt{5}}\ ,\quad \begin{Bmatrix}1&1&2\\1&1&2\\2&2&0\end{Bmatrix}=\tfrac{1}{150} \tag{A7}$$

have been used.

The terms of order m^6 are calculated analogously, this time replacing the Mayer function $\tilde{f}$ by $-\frac{1}{6}\beta^3 w_{\rm dip}^3 e^{-\beta w_{\rm LJ}}$, which results in

$$u_l^{(6)}=-\frac{2048\pi^5}{45}\left[\frac{2}{15}\right]^{1/2}\frac{(-1)^l}{(2l+1)^{3/2}}\frac{\beta^2}{\sigma^6}I_7(\beta\epsilon)\times\int d\omega\, d\omega' \Phi_{112}^3\Phi_{ll0}^* \ . \tag{A8}$$

By applying the product rule in Eq. (B8) twice the third power of Φ_{112} can also be expressed as a sum over rotational invariants:

$$\Phi_{112}^3=\left[\frac{15}{4\pi}\right]^3\sum_{\mu_1,\mu_2,\mu}\sum_{\nu_1,\nu_2,\nu}(-1)^{\nu_1+\nu_2+\nu}(2\mu_1+1)(2\mu_2+1)[(2\mu+1)(2\nu_1+1)(2\nu_2+1)]^{1/2}$$
$$\times\begin{bmatrix}1&1&\mu_1\\0&0&0\end{bmatrix}\begin{bmatrix}1&1&\mu_2\\0&0&0\end{bmatrix}\begin{bmatrix}2&2&\mu\\0&0&0\end{bmatrix}\begin{bmatrix}1&\mu_1&\nu_1\\0&0&0\end{bmatrix}\begin{bmatrix}1&\mu_2&\nu_2\\0&0&0\end{bmatrix}$$
$$\times\begin{bmatrix}2&\mu&\nu\\0&0&0\end{bmatrix}\begin{Bmatrix}1&1&2\\1&1&2\\\mu_1&\mu_2&\mu\end{Bmatrix}\begin{Bmatrix}1&1&2\\\mu_1&\mu_2&\mu\\\nu_1&\nu_2&\nu\end{Bmatrix}\Phi_{\nu_1\nu_2\nu}\ . \tag{A9}$$

After performing the integrations one has $\nu_1=\nu_2=l$, $\nu=0$, and therefore, due to the last $3j$ symbol in Eq. (A9), $\mu=2$ so that one finally obtains

$$u_l^{(6)}=-80\pi\sqrt{\tfrac{3}{7}}(2l+1)^{-1/2}\frac{\beta^2}{\sigma^6}I_7(\beta\epsilon)\sum_{\mu_1,\mu_2}(2\mu_1+1)(2\mu_2+1)\begin{bmatrix}1&1&\mu_1\\0&0&0\end{bmatrix}\begin{bmatrix}1&1&\mu_2\\0&0&0\end{bmatrix}\begin{bmatrix}1&\mu_1&l\\0&0&0\end{bmatrix}$$
$$\times\begin{bmatrix}1&\mu_2&l\\0&0&0\end{bmatrix}\begin{Bmatrix}1&1&2\\1&1&2\\\mu_1&\mu_2&2\end{Bmatrix}\begin{Bmatrix}1&1&2\\\mu_1&\mu_2&2\\l&l&0\end{Bmatrix}, \tag{A10}$$

where the values $\left(\begin{smallmatrix}220\\000\end{smallmatrix}\right)=1/\sqrt{5}$ and $\left(\begin{smallmatrix}222\\000\end{smallmatrix}\right)=-\sqrt{\frac{2}{35}}$ have been used. Due to the first two $3j$ symbols μ_1 and μ_2 must be 0 or 2 and thus $l=1,3$. For these two cases the evaluation of the sums gives

$$u_1^{(6)}=-\frac{16\pi}{225}\frac{\beta^2}{\sigma^6}I_7(\beta\epsilon)\ ,\quad u_3^{(6)}=-\frac{16\pi}{25\,725}\frac{\beta^2}{\sigma^6}I_7(\beta\epsilon)\ . \tag{A11}$$

The values for the occurring $3j$ and $9j$ symbols are obtained from the computer program MATHEMATICA.

In a completely analogous way the contributions of order m^8 are found to be

$$u_l^{(8)}=-\frac{8192}{675}\pi^{13/2}\frac{(-1)^l}{(2l+1)^{3/2}}\frac{\beta^3}{\sigma^9}I_{10}(\beta\epsilon)\int d\omega\, d\omega'\Phi_{112}^4\Phi_{ll0}^*$$
$$=-300\pi\sqrt{5}\frac{(-1)^l}{(2l+1)^{1/2}}\frac{\beta^3}{\sigma^9}\sum_{\mu_1,\mu_2,\mu}\sum_{\nu_1,\nu_2}(2\mu_1+1)(2\mu_2+1)(2\mu+1)(2\nu_1+1)(2\nu_2+1)$$
$$\times\begin{bmatrix}1&1&\mu_1\\0&0&0\end{bmatrix}\begin{bmatrix}1&1&\mu_2\\0&0&0\end{bmatrix}\begin{bmatrix}2&2&\mu\\0&0&0\end{bmatrix}^2$$
$$\times\begin{bmatrix}1&\mu_1&\nu_1\\0&0&0\end{bmatrix}\begin{bmatrix}1&\mu_2&\nu_2\\0&0&0\end{bmatrix}\begin{bmatrix}1&\nu_1&l\\0&0&0\end{bmatrix}\begin{bmatrix}1&\nu_2&l\\0&0&0\end{bmatrix}$$
$$\times\begin{Bmatrix}1&1&2\\1&1&2\\\mu_1&\mu_2&\mu\end{Bmatrix}\begin{Bmatrix}1&1&2\\\mu_1&\mu_2&\mu\\\nu_1&\nu_2&2\end{Bmatrix}\begin{Bmatrix}1&1&2\\\nu_1&\nu_2&2\\l&l&0\end{Bmatrix}, \tag{A12}$$

which results in

$$u_0^{(8)} = -\frac{8\pi}{25}\frac{\beta^3}{\sigma^9} I_{10}(\beta\epsilon) ,$$

$$u_2^{(8)} = -\frac{32\pi}{6125}\frac{\beta^3}{\sigma^9} I_{10}(\beta\epsilon) , \tag{A13}$$

$$u_4^{(8)} = -\frac{8\pi}{99\,225}\frac{\beta^3}{\sigma^9} I_{10}(\beta\epsilon) .$$

In principle, the method that leads to Eqs. (A2), (A10), and (A12) can be applied to calculate the coefficients u_l to any desired order in m. For each additional order one has in addition three summations, three $3j$ symbols and one $9j$ symbol [see Eq. (B8)]. An examination of the $3j$ symbols shows that in general the term of order m^{2n} only contributes to $u_n, u_{n-2}, \ldots, u_k$ (with $k=0$ if n is even and $k=1$ if n is odd). Thus for all l one has

$$u_l(m \to 0) \sim m^{2l} + O(m^{2l+4}) . \tag{A14}$$

APPENDIX B: PRODUCT RULE FOR ROTATIONAL INVARIANTS

In order to determine the coefficients u_l (see Appendix A) it is necessary to express a product of two rotational invariants $\Phi_{l_1 l_2 l}$ [see Eq. (2.14)] as a sum of such functions. For this purpose it is advantageous to use the $3j$ symbols [see Eq. (A.139) in [29]]

$$\begin{pmatrix} j_1 & j_2 & j \\ m_1 & m_2 & m \end{pmatrix} = (-1)^{j_1+j_2+m}(2j+1)^{-1/2} \times C(j_1 j_2 j, m_1 m_2 \overline{m}) \tag{B1}$$

instead of the Clebsch-Gordan coefficients C because of their higher symmetry. Thus we apply the form [see Eq. (2.14)]

$$\Phi_{l_1 l_2 l} = \sum_{m_1, m_2, m}{}' (-1)^{l_1+l_2+m}(2l+1)^{1/2} \times \begin{pmatrix} l_1 & l_2 & l \\ m_1 & m_2 & \overline{m} \end{pmatrix} Y_{l_1 m_1}(\omega) Y_{l_2 m_2}(\omega') Y^*_{lm}(\omega_{12}) \tag{B2}$$

and the product rule for the spherical harmonics [see Eq. (A.36) in Ref. [29]]

$$Y_{l_1 m_1}(\omega) Y_{l_2 m_2}(\omega) = \frac{1}{\sqrt{4\pi}} \sum_{l=0}^{\infty} \sum_{m=-l}^{l} (-1)^m [(2l_1+1)(2l_2+1)(2l+1)]^{1/2} \begin{pmatrix} l_1 & l_2 & l \\ 0 & 0 & 0 \end{pmatrix} \begin{pmatrix} l_1 & l_2 & l \\ m_1 & m_2 & \overline{m} \end{pmatrix} Y_{lm}(\omega) \tag{B3}$$

in order to express the product of two rotational invariants as

$$\begin{aligned} \Phi_{l_1 l_2 l} \Phi_{l_1' l_2' l'} = {} & \frac{1}{(4\pi)^{3/2}} \sum_{m_1, m_2, m}{}' \sum_{m_1', m_2', m'}{}' \sum_{\mu_1, \nu_1} \sum_{\mu_2, \nu_2} \sum_{\mu, \nu} (-1)^{l_1+l_2+l_1'+l_2'+\nu_1+\nu_2} (2l+1)(2l'+1) \\ & \times [(2l_1+1)(2l_2+1)(2l_1'+1)(2l_2'+1)(2\mu_1+1)(2\mu_2+1)(2\mu+1)]^{1/2} \\ & \times \begin{pmatrix} l_1 & l_2 & l \\ m_1 & m_2 & \overline{m} \end{pmatrix} \begin{pmatrix} l_1' & l_2' & l' \\ m_1' & m_2' & \overline{m}' \end{pmatrix} \begin{pmatrix} l_1 & l_1' & \mu_1 \\ m_1 & m_1' & \overline{\nu}_1 \end{pmatrix} \begin{pmatrix} l_2 & l_2' & \mu_2 \\ m_2 & m_2' & \overline{\nu}_2 \end{pmatrix} \begin{pmatrix} l & l' & \mu \\ m & m' & \overline{\nu} \end{pmatrix} \\ & \times \begin{pmatrix} l_1 & l_1' & \mu_1 \\ 0 & 0 & 0 \end{pmatrix} \begin{pmatrix} l_2 & l_2' & \mu_2 \\ 0 & 0 & 0 \end{pmatrix} \begin{pmatrix} l & l' & \mu \\ 0 & 0 & 0 \end{pmatrix} Y_{\mu_1 \nu_1}(\omega) Y_{\mu_2 \nu_2}(\omega') Y^*_{\mu\nu}(\omega_{12}) \end{aligned} \tag{B4}$$

with $\sum_{\mu,\nu} = \sum_{\mu=0}^{\infty} \sum_{\nu=-\mu}^{\mu}$. [Note that $m+m'-\nu=0$; see Eq. (A.130) in [29].] The summation can be considerably simplified by using the formula (A.149) in Ref. [29],

$$\sum_{\substack{m_a, m_b, m_c, m_d, \\ m_{ab}, m_{cd}}} \begin{pmatrix} l_a & l_b & l_{ab} \\ m_a & m_b & m_{ab} \end{pmatrix} \begin{pmatrix} l_c & l_d & l_{cd} \\ m_c & m_d & m_{cd} \end{pmatrix} \begin{pmatrix} l_a & l_c & l_{ac} \\ m_a & m_c & m_{ac} \end{pmatrix} \times \begin{pmatrix} l_b & l_d & l_{bd} \\ m_b & m_d & m_{bd} \end{pmatrix} \begin{pmatrix} l_{ab} & l_{cd} & l \\ m_{ab} & m_{cd} & m \end{pmatrix} = \begin{pmatrix} l_{ac} & l_{bd} & l \\ m_{ac} & m_{bd} & m \end{pmatrix} \begin{Bmatrix} l_a & l_b & l_{ab} \\ l_c & l_d & l_{cd} \\ l_{ac} & l_{bd} & l \end{Bmatrix} \tag{B5}$$

and the symmetry property

$$\begin{pmatrix} j_1 & j_2 & j \\ m_1 & m_2 & m \end{pmatrix} = (-1)^{j_1+j_2+j} \begin{pmatrix} j_1 & j_2 & j \\ \overline{m}_1 & \overline{m}_2 & \overline{m} \end{pmatrix} \tag{B6}$$

of the $3j$ symbols. The $9j$ symbol is given by [Eq. (A.291) in Ref. [29]]

$$\begin{Bmatrix} a & b & c \\ d & e & f \\ g & h & i \end{Bmatrix} = \sum_{x=0}^{\min(a+i,h+d,f+b)} (2x+1) \begin{Bmatrix} a & i & x \\ h & d & g \end{Bmatrix} \begin{Bmatrix} h & d & x \\ f & b & e \end{Bmatrix} \begin{Bmatrix} f & b & x \\ a & i & c \end{Bmatrix} . \tag{B7}$$

A lengthy explicit formula as well as certain symmetry properties for the $6j$ symbols $\{\begin{smallmatrix} a & b & c \\ d & e & f \end{smallmatrix}\}$ are given in Sec. A.5.1 of Ref. [29]. By applying Eq. (B5) to Eq. (B4) one finally obtains

$$\begin{aligned} \Phi_{l_1 l_2 l} \Phi_{l'_1 l'_2 l'} = & (-1)^{l_1+l_2+l+l'_1+l'_2+l'} (4\pi)^{-3/2} \\ & \times \sum_{\mu_1,\mu_2,\mu} [(2l+1)^2(2l'+1)^2(2l_1+1)(2l_2+1)(2l'_1+1)(2l'_2+1)(2\mu_1+1)(2\mu_2+1)]^{1/2} \\ & \times \begin{pmatrix} l_1 & l'_1 & \mu_1 \\ 0 & 0 & 0 \end{pmatrix} \begin{pmatrix} l_2 & l'_2 & \mu_2 \\ 0 & 0 & 0 \end{pmatrix} \begin{pmatrix} l & l' & \mu \\ 0 & 0 & 0 \end{pmatrix} \begin{Bmatrix} l_1 & l_2 & l \\ l'_1 & l'_2 & l' \\ \mu_1 & \mu_2 & \mu \end{Bmatrix} \Phi_{\mu_1 \mu_2 \mu} , \end{aligned} \tag{B8}$$

where Eq. (B2) and the condition $\nu_1+\nu_2-\nu=0$ have been used.

[1] D. Wei and G. N. Patey, Phys. Rev. Lett. **68**, 2043 (1992).
[2] D. Wei and G. N. Patey, Phys. Rev. A **46**, 7783 (1992).
[3] J. J. Weis, D. Levesque, and G. J. Zarragoicoechea, Phys. Rev. Lett. **69**, 913 (1992).
[4] J. J. Weis and D. Levesque, Phys. Rev. E **48**, 3728 (1993).
[5] L. Onsager, Proc. N.Y. Acad. Sci. **51**, 627 (1949).
[6] D. Frenkel, in *Liquids, Freezing and Glass Transition,* Proceedings of the Les Houches Summer School of Theoretical Physics, Les Houches, 1991, Session LI, edited by J. P. Hansen, D. Levesque, and J. Zinn-Justin (Elsevier, Amsterdam, 1991), p. 689.
[7] M. Born, Sitz., Phys. Math. **25**, 614 (1916); Ann. Phys. (Leipzig) **55**, 221 (1918).
[8] J. Prost, R. Bruinsma, and F. Tournilhac, J. Phys. II **4**, 169 (1994).
[9] R. B. Meyer, L. Liébert, L. Strzelecki, and P. Keller, J. Phys. (Paris) Lett. **36**, L69 (1975).
[10] D. Wei, G. N. Patey, and A. Perera, Phys. Rev. E **47**, 506 (1993).
[11] K. Sano and M. Doi, J. Phys. Soc. Jpn. **52**, 2810 (1983).
[12] H. Zhang and M. Widom, J. Magn. Magn. Mater. **122**, 119 (1993).
[13] M. Kinoshita and M. Harada, Mol. Phys. **79**, 145 (1993).
[14] M. Kasch and F. Forstmann, J. Chem. Phys. **99**, 3037 (1993).
[15] J.-M. Caillol, J. Chem. Phys. **98**, 9835 (1993).
[16] M. E. van Leeuwen and B. Smit, Phys. Rev. Lett. **71**, 3991 (1993).
[17] R. E. Rosensweig, Sci. Am. **247** (4), 124 (1982); *Ferrohydrodynamics* (Cambridge University Press, Cambridge, England, 1985).
[18] P. Frodl and S. Dietrich, Phys. Rev. A **45**, 7330 (1992); Phys. Rev. E **48**, 3203 (1993).
[19] P. Frodl and S. Dietrich, Phys. Rev. E **48**, 3741 (1993).
[20] S. W. de Leeuw, J. W. Perram, and E. R. Smith, Proc. R. Soc. London Ser. A **373**, 27 (1980); **388**, 177 (1983).
[21] B. Groh and S. Dietrich, Phys. Rev. Lett. **72**, 2422 (1994).
[22] J. A. Barker and D. Henderson, J. Chem. Phys. **47**, 4714 (1967).
[23] J. D. Weeks, D. Chandler, and H. C. Andersen, J. Chem. Phys. **54**, 5237 (1971).
[24] J. P. Hansen and I. R. MacDonald, *Theory of Simple Liquids* (Academic, London, 1976).
[25] G. Stell, J. C. Rasaiah, and H. Narang, Mol. Phys. **23**, 393 (1972); **27**, 1393 (1974).
[26] N. F. Carnahan and K. E. Starling, J. Chem. Phys. **51**, 635 (1969).
[27] J. A. Barker and D. Henderson, J. Chem. Phys. **47**, 2856 (1967).
[28] M. E. Rose, *Elementary Theory of Angular Momentum* (Wiley, New York, 1957).
[29] C. G. Gray and K. E. Gubbins, *Theory of Molecular Fluids* (Clarendon, Oxford, 1984).
[30] P. M. Levy and D. P. Landau, J. Appl. Phys. **39**, 1128 (1968); P. M. Levy, Phys. Rev. **170**, 595 (1968).
[31] J. A. Stratton, *Electromagnetic Theory* (McGraw-Hill, New York, 1941).
[32] R. Becker and F. Sauter, *Theorie der Elektrizität* (Teubner, Stuttgart, 1973), Vol. 1.
[33] W. F. Brown, Jr., in *Dielektrika,* edited by S. Flügge, Handbuch der Physik Vol. XVII (Springer, Berlin, 1956), p. 1.
[34] I. D. Lawrie and S. Sarbach, in *Phase Transitions and Critical Phenomena,* edited by D. C. Domb and J. L. Lebowitz (Academic, London, 1984), Vol. 9, p. 1.
[35] D. Marx, P. Nielaba, and K. Binder, Phys. Rev. Lett. **67**, 3124 (1991).
[36] S. Sengupta, D. Marx, and P. Nielaba, Europhys. Lett. **20**, 383 (1992).
[37] P. de Smedt, P. Nielaba, J. L. Lebowitz, J. Talbot, and L. Dooms, Phys. Rev. A **38**, 1381 (1988).
[38] R. B. Griffiths, Phys. Rev. **176**, 655 (1968).
[39] M. Widom and H. Zhang (unpublished).
[40] B. Groh and S. Dietrich (unpublished).
[41] H. Zhang and M. Widom, Phys. Rev. E **49**, 3591 (1994).
[42] P. G. de Gennes and P. A. Pincus, Solid State Commun. **7**, 339 (1969).
[43] P. G. de Gennes and P. A. Pincus, Phys. Kondens. Mater. **11**, 189 (1970).

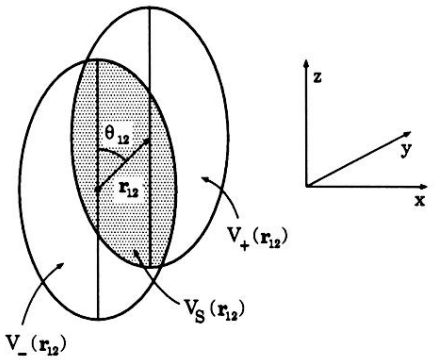

FIG. 1. Illustration of the regions of integration in Eq. (3.5). For an ellipsoidal sample and a fixed vector difference $\mathbf{r}_{12}$ the vector sum $\mathbf{r}_S$ lies in the shaded volume $V_S(\mathbf{r}_{12})$ given by the intersection $V_+(\mathbf{r}_{12}) \cap V_-(\mathbf{r}_{12})$ of two ellipsoids.

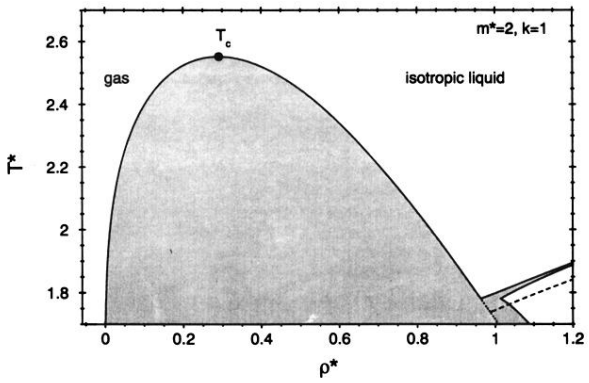

FIG. 11. Phase diagram for a spherical sample ($k=1$). The formation of a ferroelectric phase affects the phase diagram only at very high densities where a weakly first-order transition between the isotropic and ferroelectric liquid is found, which extends up to the highest densities considered. The dashed line denotes the absolute stability limit of the isotropic phase given by Eq. (7.10), which represents the analytic continuation of $\rho_{fc}(T)$ (compare Figs. 5 and 9).

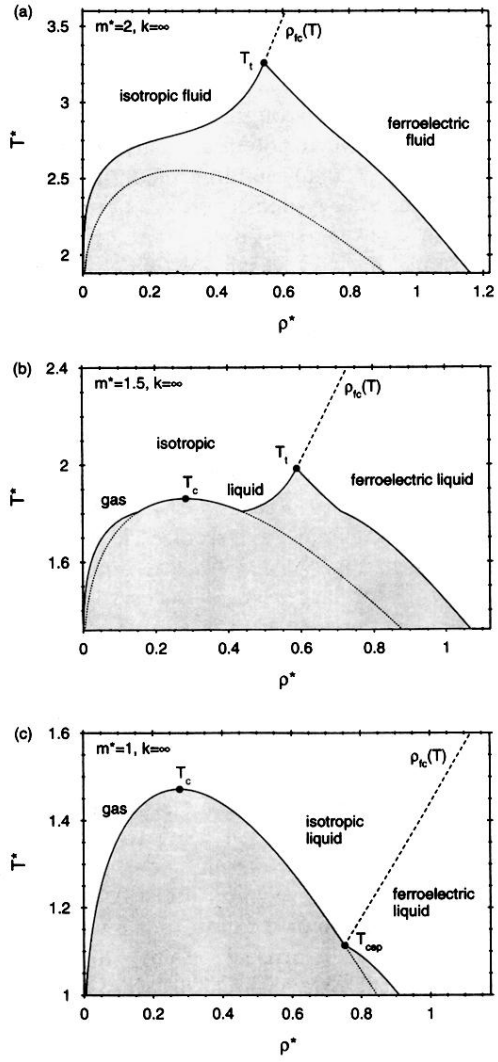

FIG. 15. Phase diagrams for needle-shaped samples ($k \to \infty$) with reduced dipole moments (a) $m^* = 2$, (b) $m^* = 1.5$, and (c) $m^* = 1$. T_{cep} denotes a critical end point. For more details see the main text.

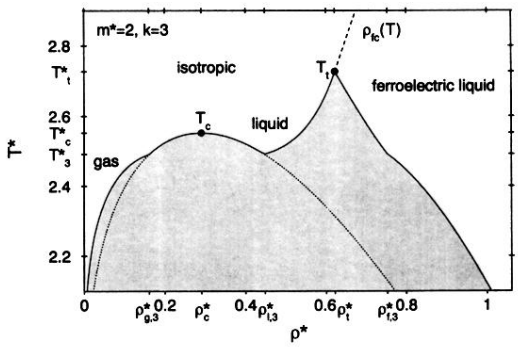

FIG. 5. Phase diagram for the dipole moment $m^*=2$ and the aspect ratio $k=3$. Below the triple temperature T_3 a ferroelectric liquid coexists with an isotropic gas. Between T_3 and the critical temperature T_c there are three possible phases: an isotropic gas, an isotropic liquid, and a ferroelectric liquid. The first-order phase transition between the isotropic and the ferroelectric liquid turns into a second-order phase transition at the tricritical temperature T_t. Above T_t there is a line of critical points $\rho_{fc}(T)$ given by the dashed curve. The dotted lines denote the two phase region of the isotropic gas and the liquid if the ferroelectric phase is not taken into account. Within the shaded region there are no thermodynamically stable states. At high densities the system freezes. The corresponding solid phase is not shown because it is not accessible by the present theory.

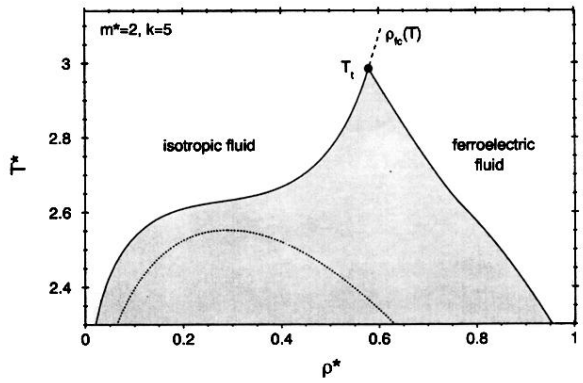

FIG. 9. Phase diagram for $m^*=2$ and $k=5$ exhibiting only two phases, an anisotropic fluid at low densities and a ferroelectric fluid at high densities. The dashed line $\rho_{fc}(T)$ indicates the line of second-order phase transitions above the tricritical temperature T_t. As in Fig. 5 the dotted curve is the phase diagram if the ferroelectric phase is not taken into account. Within the shaded region there are no thermodynamically stable states. Note that in comparison to Fig. 5 the critical point T_c has disappeared. The solid phase is missing.